Jaime Moreira Machado Faria

Licenciatura em Engenharia de Micro e Nanotecnologias

Production and optimization of hybrid fibrillary gels by colloidal electrospinning

Dissertação para Obtenção do Grau de Mestre em
Engenharia de Micro e Nanotecnologias

Orientador: Doutora Coro Echeverria Zabala, Investigadora em Pós-doutoramento, CENIMAT-I3N Departamento de Ciência dos Materiais, Faculdade de Ciências e Tecnologia da Universidade Nova de Lisboa

Co-orientador: Doutora Paula Isabel Pereira Soares, Investigadora em Pós-doutoramento, CENIMAT-I3N Departamento de Ciência dos Materiais, Faculdade de Ciências e Tecnologia da Universidade Nova de Lisboa

Júri

Presidente: Doutor Rodrigo Ferrão Paiva Martins, Professor Catedrático, FCT-UNL

Arguente: Doutor Jorge Alexandre Monteiro Carvalho Silva, Professor Auxiliar, FCT-UNL

Vogal: Doutora Coro Echeverria Zabala, Investigadora em Pós-doutoramento, FCT-UNL

Outubro de 2016

FACULDADE DE CIÊNCIAS E TECNOLOGIA
UNIVERSIDADE NOVA DE LISBOA

Production and optimization of hybrid fibrillary gels by colloidal electrospinning

Para o meu Avô Quito

“Break the cycle. Rise above. Focus on science”

Rick Sanchez

Acknowledgments/Agradecimentos

Agradeço à minha orientadora, Doutora Coro Echeverria Zabala, não só pela ajuda prestada na parte experimental, mas também pelas muitas correções na parte escrita. Obrigado por me teres mostrado que é preciso tratar os microgéis e o electrospinning com muito amor e carinho, algo que eu às vezes não tinha. Sei que na reta final posso ter tremido um bocadinho, mas agradeço por estares sempre presente e insistir que se precisasse de alguma ajuda bastava chamar. Obrigado também por todas as palavras de apoio e de encorajamento, especialmente aquelas que vinham em "portunhol".

À minha co-orientadora, Doutora Paula Soares, obrigado por teres sido exigente comigo quando eu preguiçava, mas por também me teres dado descanso quando vias que estava à beira de bater com a testa no chão. Obrigado por me teres mostrado que, apesar das confusões que eu escrevi nas primeiras versões da tese, eu sabia o que devia dizer mas simplesmente metia os pés pelas mãos. Agradeço também toda a magia que fizeste na altura das formatações: sem elas, algumas das imagens ainda seriam só 4 píxeis.

Ao Professor João Paulo Borges um grande obrigado por toda a ajuda dada durante a tese, não só na parte do electrospinning, mas também em pequenas dúvidas que iam surgindo pelo caminho. Agradeço ainda por me ter dado a oportunidade de realizar/orientar algumas atividades que decorreram no laboratório de Biomateriais no âmbito da ExpoFCT e da Ciência Viva. Foram experiências sem dúvida memoráveis e enriquecedoras.

À Doutora Susete Fernandes, um grande obrigado pela ajuda dada na parte final da tese, ainda que os resultados não tenham sido os melhores. Obrigado também pelas palavras de apoio ditas durante esta etapa.

Ao Mestre Carlos João (quase Doutor!!) por todos os momentos de boa disposição no laboratório e por me relembrar que quando se joga *Street Fighter* há que escolher sempre o Ryu.

À Maria Augusta, obrigado por aquelas míticas manhãs de quizomba e por todos os bons momentos com gargalhadas sem fim no laboratório.

Ao Doutor Rodrigo Martins e à Doutora Elvira Fortunato, agradeço por terem criado este magnífico curso e por o terem estruturado de maneira a que os alunos que o concluem tenham conhecimento, não só experimental mas também académico, para vingar como investigadores internacionais.

À Susana, obrigado por toda a ajuda prestada, desde artigos recomendados a dicas sobre como fazer as experiências de electrospinning de uma maneira fácil, rápida e eficaz. Obrigado também por teres apertado comigo no início quando eu ainda estava com ideia que tinha tempo para tudo.

À Joana, por apesar de já estares despachada da tese ias ter ao laboratório a ver se eu ainda não tinha rebentado. Obrigado pela ajuda no electrospinning, nos magníficos ensaios de tração e por aquele milagroso Excel que muito tempo me poupou.

Às minhas amigas do laboratório de polímeros – Ana, Gabriela, Inês, Mariana e Tânia – obrigado por todos os bons momentos de descompressão e pela paciência que tiveram nos meus maus momentos. Agora é altura de fazer das palavras favoritas da Tânia minhas: "Vou abandonar, tenho uma consulta às 5".

Ao Ribas e ao Minhoca, obrigado por todas as animes, *light novels*, jogos, *posts* do 9 gag, imagens do imgur e muitas outras coisas que não podem ser aqui mencionadas. Sem dúvida foram essenciais para me abstrair e relaxar quando a cabeça já não aguentava.

À Caupers e à Marta, obrigado por tentarem fazer com que eu "trabalhasse" quando a minha vontade era não o fazer (e obrigado pelos magníficos gifs dos gatinhos). Apesar de não mostrarem, eu sei que no fundo, no fundo, no fundo até que gostam da minha pessoa.

Ao Vasco, obrigado por me avisares quando um Pikachu mandava *spawn* no DQ e por me desencaminhares em inúmeras caças a estes bichos que quase desgraçaram uma tese. Agradeço também à Cátia por dar nas orelhas do Vasco quando ele não me deixava trabalhar.

À tropa da Teresa (Trigo, Monteiro, Bártolo, Tomás e Luka), obrigado por todas as tardes bem passadas com cartadas e sumo de cevada.

À Ana, que me acompanhou desde o primeiro dia de laboratório e que preveniu que eu virasse maluquinho. Obrigado por todos os almoços, cafés de 1h30 e lanches. Chegámos ao fim sãos, quem diria.

À Chamiço, obrigado pelas piadas, risos e discussões sem sentido (que nesta altura foram mais que as normais, curioso…). Ainda não foi desta que fui a uma das míticas festas, mas sei que há alguma para breve.

Ao Farinha (Sr. Engenheiro), obrigado por estares sempre disponível quando um gajo precisava de tirar uma dúvida, fosse do que fosse. Eu sei que tentaste que percebêssemos quântica, mas há batalhas que não podem ser ganhas.

À Andreia, que começou a tese em França a mas apercebeu-se que os *avecs* não eram tão bons quanto os migos dela, obrigado pelo apoio e motivação que me deste nesta última parte.

Ao Bernardo (Benny Benassi), obrigado pelo apoio e pelos momentos de parvoíce e descompressão. As sessões de trabalho de tese em tua casa podem não ter rendido muito, mas ao menos comemos bons croissants de chocolate e donuts (apesar daquele leite já ter visto melhores dias).

À Carolina (a.k.a., o piolho), obrigado por me estares sempre a dar nas orelhas e a apertar comigo para ver se eu despachava a tese a tempo e horas. Agradeço também por sempre te mostrares disponível para me ajudar no trabalho laboratorial, apesar de nunca te ter pedido que o fizesses. Obrigado por todo o apoio, e espero que saibas que se precisares de alguma coisa, basta apitares.

À Sofia, obrigado por todas as conversas, desabafos e pausas para café que fazíamos para parar de pensar neste bicho-de-sete-cabeças a que chamamos tese. Apesar de teres ido fazer a tese para fora e teres ficado fora de vista, nunca ficaste longe do coração.

Ao Zé, obrigado por todas as viagens de 158 com boa companhia e por estares presente tanto nos bons como nos maus momentos, fossem eles da tese ou de alguma outra coisa. Podemos não ter entrado ao mesmo tempo, mas ainda bem que pude partilhar os stresses da tese e acabá-la contigo.

Ao Gonçalo, agradeço o apoio dado e todos aqueles sons de *old-school Drum&Bass* relembrados e partilhados. Ainda não foi desta que vimos Karetus, mas pode ser que no próximo Crato eles decidam aparecer e dê para ficarmos até às quinhentas a partir chão.

À Ana (a pessoa que mais chateia o Minhos), obrigado por todas as manhãs, tardes, noites e fins-de-semana de trabalho na 202. Apesar de não termos tido sorte a PAFEND, das tuas incessantes tentativas de nos levares a almoçar ao restaurante de luxo e dos teus pedidos constantes de "coça-coça migo!", ainda bem que tive a oportunidade de fazer isso tudo contigo, a minha chata máxima.

À Carolina (a nossa prima ballerina), obrigado por todo o apoio e carinho que me deste durante a faculdade inteira. Eu sei que algumas vezes podemos não ter estado do meu lado, ou mesmo termos achado que a outra pessoa estava a ser má ou a agir mal, mas no final de contas tudo o que nos faltava era uma cervejita na mão para acalmar os nervos e uma boa tarde de palheta.

Agradeço aos meus Pussies (Almeida, Bruno, Daniel, Gabriel e Pinto), que estão comigo desde o princípio e que sem eles nada disto fazia sequer sentido. Ao Almeida (Princesa), obrigado por todas as memoráveis noites de festa na FCT (e uma ou outra em branco), por todos os *gins*, cervejas e *shots* de tequila; obrigado por todas as discussões que tivemos, fossem elas sobre matéria ou simplesmente sobre o porquê de o céu ser azul; e graças a

deus pela tua magnífica autocaravana, salvadora de sonos e *shit-faces*. Ao Bruno (Gostoso), o primeiro veterano que conheci quando entrei, obrigado por todo o apoio, amor incondicional e carinho mostrados durante estes anos. Teremos sempre aquele mítico relatório de Micro II, que inclusive trouxe uma lágrima de alegria ao Luís Pereira (assumo eu). Ao Daniel (Dan-Dan), obrigado por todas as palavras de força e confiança e por todos os momentos partilhados nas praxes, jantares, desfile e afins. Digo com confiança que até hoje não tivemos melhor aula que aquela prática de Análise I com o Phelps a imitar gorilas como se não houvesse amanhã. Ao Gabriel (Gato), que até hoje ainda não sabe falar Português como deve ser (mas isso é outra batalha), obrigado por todos os bons e maus momentos que passámos juntos e pelos dias passados no Tico a contemplar a vida. Uma grande mente uma vez disse: *get schwifty*; acho que ao fim deste tempo todo, conseguimos. Ao Pinto (my brother from another mother), obrigado por todas as passagens de ano, férias, conversas de café e muito mais que agora não me recordo. Foram 6 anos… 6 anos de histórias impossíveis de resumir numas míseras linhas, mas se o tiver fazer: insubstituível.

Por último, mas mais importante, quero expressar o meu enorme agradecimento à minha mãe, ao meu pai e ao meu irmão (que na realidade só me chaga o juízo, mas faz parte) que sempre me apoiaram e aturaram nos momentos de mau feitio. Obrigado por toda a compreensão que tiveram, por me perguntarem sempre como tinha corrido o dia, mesmo vendo pela minha cara que não tinha corrido bem, e por me relembrarem que às vezes descansar é melhor que continuar a insistir.

Sem todos vocês, esta tese seria uma mera página em branco em cima da minha secretária. Obrigado.

Abstract

Electrospinning technique has proven to be a suitable approach to produce high surface area to volume ratio polymeric membranes with tailored architecture. To increase its functionality, a straightforward strategy can be the confinement of externally stimuli responsive systems, such as microgels. This combination enables the production of multifunctional composite systems.

This thesis reports the development of composite fibres through colloidal electrospinning constituted by polyvinylpyrrolidone (PVP) containing poly(N-isopropylacrylamide) (PNIPAAm) microgels. The focus of the dissertation deals with the optimization of the fibre precursor, PVP. In the first stage, an extensive study towards the production of PVP non-woven mats with high surface area to volume ratio was performed. The obtained non-woven mats were crosslinked using UV irradiation, a green and cost-effective technique, to ensure structure stability in the presence of a solvent (prevent dissolution). Non-woven mats were further characterized in terms of morphological, mechanical and swelling properties. In addition, the fibre precursor, PVP, was analysed through a process-dependent comparative study: non-woven mats vs. films. The most suitable electrospinning parameters were further used to confine PNIPAAm thermoresponsive microgels in PVP fibres through colloidal electrospinning. The system was further crosslinked and fully characterized to obtain a multiresponsive composite system.

This versatile approach is a starting point to design and produce composite multifunctional systems that could be tailored for a wide range of applications.

KEYWORDS: PVP; PNIPAAm; Composites; Microgels; Colloidal Electrospinning; Fibers

Resumo

A electrofiação tem-se destacado como uma técnica bastante vantajosa na produção de membranas poliméricas de elevada razão área superficial/volume com estruturas programáveis. De modo a aumentar a funcionalidade, a incorporação de sistemas que respondem a estímulos externos, como os microgéis, evidencia-se como uma técnica relativamente simples. Ao incorporar microgéis em fibras poliméricas é possível criar sistemas compósitos multifuncionais.

Esta tese reporta o desenvolvimento de fibras compósitas de polyvinylpyrrolidone (PVP) contendo microgéis de poly(*N*-isopropylacrylamide) (PNIPAAm) através da técnica de electrofiação coloidal. O foco da tese centra-se na otimização do formador de fibra, PVP. Numa primeira fase foi feito um estudo intensivo de modo a obter fibras de PVP monodispersas com elevada razão área superficial/volume. As membranas obtidas foram reticuladas com radiação UV – técnica sustentável e de baixo custo – de modo a garantir a estabilidade da rede na presença de um solvente (evitar dissolução). As membranas foram ainda caracterizadas por meio de testes mecânicos e de inchamento, bem como analisadas a nível morfológico. De referir que as propriedades do PVP foram analisadas através de um estudo comparativo baseado no método de produção: membranas *vs.* filmes. Os parâmetros de electrofiação mais adequados foram utilizados na incorporação de microgéis termosensíveis de PNIPAAm em fibras de PVP com recurso à técnica de electrofiação coloidal. O sistema foi reticulado e caracterizado de modo a se obter um sistema compósito capaz de responder a diferentes estímulos.

Esta abordagem, para além de versátil, é o ponto de partida para o desenvolvimento e produção de sistemas compósitos multifuncionais ajustáveis para um vasto leque de aplicações.

Palavras-chave: PVP; PNIPAAm; Compósitos; Microgéis; Electrofiação Coloidal; Fibras

Contents

List of Figures

List of Tables

Abbreviations

AAc	Acrylic Acid
APS	Ammonium Persulfate
ATR	Attenuated Total Reflectance
Cs	Chitosan
DLS	Dynamic Light Scattering
EtOH	Ethanol
FIB	Focused Ion Beam
FTIR	Fourier transform infrared
HEMA	Hydroxyethylmethacrylate
LCST	Lower Critical Solution Temperature
MBA	*N,N*-methylene bis-acrylamide
MFD	Mean fibre diameter
MG	Microgel
MG6AAc	Poly(*N*-vinylpyrrolidone) microgel with 6 wt.% of Acrylic acid
MG10AAC	Poly(*N*-vinylpyrrolidone) microgel with 10 wt.% of Acrylic acid
PEO	Poly(ethylene oxide)
PNIPAAm	Poly(*N*-isopropylacrylamide)
PVP	Polyvinylpyrrolidone
RH	Relative Humidity
SBS	Sodium Bisulphite
SEM	Scanning Electron Microscopy
SFEP	Surfactant Free Emulsion Polymerization
TCD	Tip-to-collector distance
TEM	Transmission Electron Microscopy
UTS	Ultimate Tensile Strength
UV	Ultraviolet
VPTT	Volume Phase Transition Temperature

Symbols

ρ_x	Crosslinking density
ε	Elongation at break
C_n	Flory characteristic ratio
χ_1	Flory interaction parameter
l	Length of the bond along the polymer's backbone
t_{swell}	Maximum swelling capability time
ξ	Mesh size
V_1	Molar volume of water
$\overline{M}_c$	Molecular weight of the polymer chain between two neighbouring crosslinking nodes
$\overline{M}_n$	Molecular weight of the polymer chains prepared without a crosslinker
M_r	Molecular weight of the repeating units
$\upsilon_{2,s}$	Polymer volume fraction in the swollen state
$\bar{\upsilon}$	Specific volume of the polymer
τ	Tortuosity
$\upsilon_{2,r}$	Volume fraction of the chains in the relaxed state
λ	Wavelength
W_d	Weight of the film/non-woven mat prior to immersion
W_s	Weight of the film/non-woven mat after immersion
E	Young's Modulus

Motivation and Objectives

The development of new materials/systems that can be tailored for a specific application has always been a topic of interest in materials research. Within a variety of systems, microgels stand out due to their simplicity and versatility. For instance, poly(*N*-isopropylacrylamide) (PNIPAAm) microgels – which are thermosensitive by nature – when combined with other components can respond to further stimuli such as light and magnetic fields [1, 2].

Furthermore, if we confine microgels inside structures with a high surface to volume ratio as well as high porosity – polymeric electrospun fibres – we can develop not only composite systems that have surfaces with tailored morphologies, but also increase the entire system sensitivity due to the individual properties of each element in the composite.

In the Soft and Biofunctional Materials (SBM) research group, microgels and their confinement inside electrospun fibres are topics that have been explored. In a first work, the preparation of multi-stimuli lower critical solution temperature (LCST)-like magnetic hybrid microgels was reported [3]. The reported microgels successfully maintained the swelling ability of PNIPAAm microgels (LCST ~32 ºC) and preserved the magnetic properties of iron oxide nanoparticles. Marques *et al.* reports the synthesis and optimization of PNIPAAm/Chitosan stimuli-responsive microgels and further confinement inside poly(ethylene oxide) (PEO)/Water/Ethanol (EtOH) electrospun fibres [4]. The PNIPAAm/Chitosan microgels presented a volume phase transition temperature (VPTT) of approximately 37ºC (for the highest concentration of chitosan) and were successfully confined inside 63 ± 25 nm electrospun fibres, which presented a 'bead-on-a-string' morphology.

Although both works report the successful synthesis of microgels, each presented their own drawbacks. For instance, the microgels reported in [3] present a LCST of approximately 32ºC, which is not suitable for physiological applications where the work temperature is around 37ºC. Besides, the fibre template used for the production of the electrospun composite system was water soluble, which makes it unsuitable for physiological applications [4].

The objective of the present work is the development of composite fibres able to form membranes with potential to tune its surface wettability. We report the study and optimization of poly(*N*-vinylpyrrolidone) (PVP) as the fibre template for the production of said composite membranes. A UV irradiation treatment was applied to the PVP non-woven mats in order to ensure structure stability in the presence of a solvent (prevent dissolution). Later on, an attempt to confine PNIPAAm-Acrylic acid (AAc) microgels was made – acrylic acid was used to increase the microgels' LCST to more physiological values – so to develop a proof of concept of a UV crosslinked composite multifunctional system that could be used as a controlled release mechanism, self-healing, filter, among others.

Concerning the optimization of PVP as fibre template, several studies were performed in order to find the optimal electrospinning parameters and UV irradiation times with the final goal of obtaining a membrane that could not only present a somewhat elastic behaviour but also maintain its structural stability. This topic involved the following studies:

- Study the influence of electrospinning parameters, such as polymer concentration, process flow-rate, applied voltage and tip-to-collector distance in the resulting non-woven mats;
- Comparative study of non-woven mats vs. films to evaluate the morphological, mechanical and swelling properties of PVP and respective variation with UV irradiation time.

For the development of the composite multifunctional system, this topic was divided into the following sub-objectives:

- Synthesis and characterization of PNIPAAm-AAc microgels;
- Production of composite membranes using a simple, cost-effective and versatile technique – Colloidal Electrospinning;
- Study of morphological, mechanical and swelling properties of the composite membranes in order to understand the influence of the confined microgels in the overall system.

1 Introduction

1.1 Composite materials

Materials engineering has always focused on the assembly of materials with enhanced properties that can serve multiple purposes. By combining two or more physically and/or chemically distinct materials, a new product with characteristics that are not presented by any of its components in their isolated stated can be manufactured. These 'new' materials are commonly called composite materials [5].

The applications of composite materials are not limited to the automotive or aircraft industries [6-8].Composite materials are necessarily multifunctional materials, and the strong growth in the use of composites has been greatly influenced by multifunctional design requirements [9]. Over the last years, research has been made in order to produce systems that can release drugs [10, 11] or even self-heal [12] when in presence of a specific stimuli. For instance, Ke *et al* reported on the production of a novel smart system based on poly(D,L-lactic-*co*-glycolic acid) (PLGA) hollow microspheres that can deliver anticancer drug into tumour cells using the change in pH values of the tumour cell as the triggering stimulus [10].

When considering the production method of these stimuli-responsive multifunctional systems, electrospinning technique comes as an advantage since it not only enables the facile incorporation of the active sites [13], but also enhances the sensitivity of the entire system to external stimuli due to the extremely large surface area and porosity of the fibres (polymeric matrix) [14, 15].

1.2 Colloidal Electrospinning

Electrospinning is a cost-effective, simple and versatile process capable of forming polymer fibres in the submicron range with high surface to volume ratio, flexibility and tuneable porosity [16, 17]. This process works by applying a high electric field to the droplet of a fluid – solution or melt – that is coming out from the tip of a needle, which acts as one of the electrodes. The electric field leads to the droplet's deformation and posterior ejection from the tip of the cone in the form of a charged jet, which is then accelerated towards a counter-electrode, leading to the formation of continuous fibres [16]. The fibres resulting from the electrospinning process have been used in a variety of applications, ranging from sensors to drug delivery and tissue scaffolds [18-21].

Although electrospinning is a simple process, the fibre's surface topography, morphology and orientation are highly dependent on a number of parameters, which can be grouped in three different categories: i) solution parameters, ii) process parameters and iii) environmental conditions [17]. For instance, when the polymer's concentration is very low its viscosity is not enough to guarantee the entanglement of the polymeric chains, phenomenon required for fibre formation. This leads to 'electrospraying', which results in the formation of particles instead of fibres [22]. Other parameters, such as flow rate, applied voltage, tip-to-collector distance and relative humidity have great influence on the electrospinning process. Those will be further studied and discussed in Section 3.1.1.

Colloidal or emulsion electrospinning is a technique similar to the traditional electrospinning but uses a colloidal system of two or more immiscible phases as fibre precursor, instead of a homogeneous solution [23]. Since this technique allows the production of multicomponent nanofibres with controlled morphology using a simple nozzle, colloidal electrospinning comes as a good replacement for co-axial electrospinning, which uses coaxial nozzles for

the same purpose [24]. Moreover, co-axial electrospinning does not guarantee the production of core-shell fibres due to the influence of the flow rate of the inner and outer solutions and the viscoelasticity of the polymers involved [25]. Furthermore, this approach is environmentally friendly since it enables the minimization of the amount of organic solvents used during the production process [26]. Figure 1.1 depicts a colloidal solution and how the different components interact in order to form a core-shell fibre.

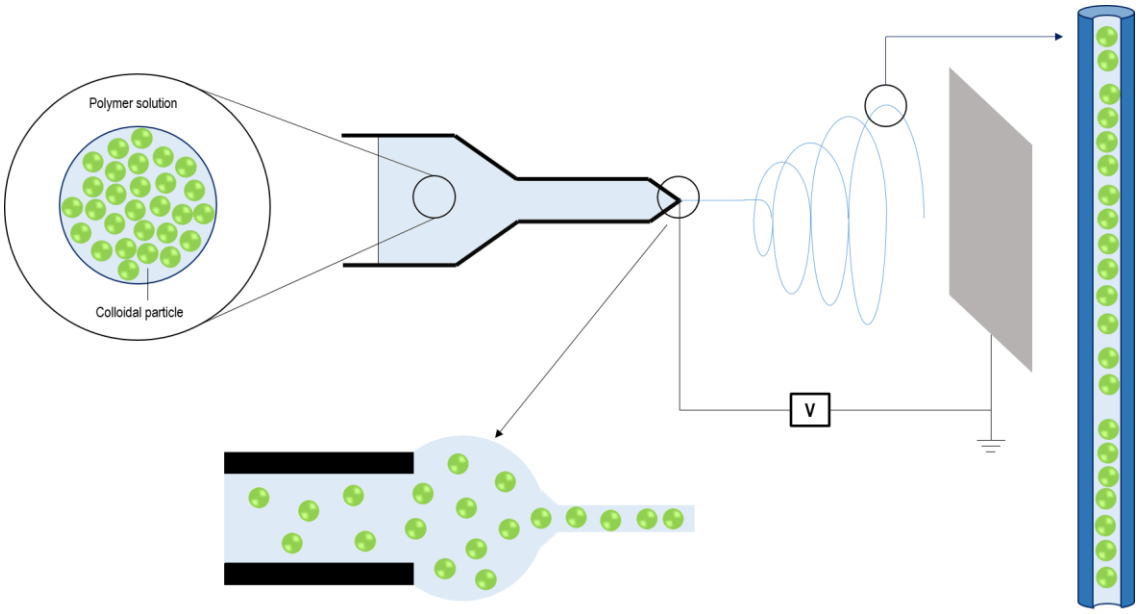

Figure 1.1 – Schematic illustration of a colloidal electrospinning set-up. The green circles represent the colloidal phase, which can be either organic or inorganic compounds. (Adapted from [13])

One of the main advantages that colloidal electrospinning possesses is the different fibre morphologies that can be obtained, regarding dispersed phase placement inside the fibre. Taking this in consideration, there are two main types of morphologies that appear in colloidal electrospinning fibres: 'bead-on-a-string' [27] and 'core-shell' [28]. In order to best comprehend these morphological structures, it is necessary to consider the dispersed phase evolution during the electrospinning process [29]. Regarding the 'bead-on-a-string' structures, when the emulsion flows through a long capillary and forms the expected accelerated bending fluid jets, the dispersed phase has the tendency to accumulate in the centre of the liquid along the direction of fluid during its flight in the air. This helps the microbeads to settle in the centre of the fibre, rather than on the surface [27]. If the electric field is too high, the beads will suffer higher elongation, displacing them from the centre and making them settle closer to the fibre's surface, giving rise to 'spindle-like' structures [27]. As for the core-shell fibres, the viscosity difference between the particles and the polymeric matrix – core and shell respectively – plays an important role. During the electrospinning process, the particles are stretched into elliptical shapes in the fibre's axial direction, giving rise to a continuous core [30]. If the viscosity of the particles vs. viscosity of the polymer matrix is not correct, particles do not fully elongate and break up, leading to the formation of beads instead of a continuous core [30, 31].

Due to their morphology, colloidal electrospinning core-shell fibres are widely used as carriers for drug or biological agents. These systems can be produced using either a mixture of drug emulsifier in a polymer solution [27] or an emulsion core spinning with a polymer solution acting as the shell [30]. One option is to incorporate stimuli-sensitive

microgels, which can act as drug carriers, into polymeric fibres by means of colloidal electrospinning. This set-up would originate multifunctional fibres with fast thermosensitive behaviour and tuneable surfaces. Few studies report the confinement of microgels inside polymeric fibres. Díaz *et al.* produced composite fibres of PNIPAAm-based microgels using PVP as fibre template, obtaining fibres with a mean diameter of 0.9 μm and a water uptake of 17 times their dry weight [32]. PEO fibres with confined PNIPAAm-chitosan (PNIPAAm-Cs) microgels with a mean diameter of 63 nm and bead-on-a-string morphology were reported by Marques *et al.* [4].

1.3 Thermosensitive microgels

Microgels are intramolecular crosslinked polymer particles of colloidal size (10 – 1000 nm) that swell in the presence of a suitable solvent [3, 33, 34]. Depending on their composition, the interactions with the solvent can be triggered/controlled *via* external stimuli, such as temperature, pH, magnetic and electric field and even light. This feature makes polymeric microgels materials of interest for biomedicine, sensing and imaging applications [35-38].

Thermosensitive microgels are colloidal particles that undergo a conformational change under a specific temperature range, when in contact with suitable solvents. One of the most studied is a negative temperature-sensitive polymer called PNIPAAm, which has a transition temperature, in aqueous medium, near human body temperature (~ 32 ºC). This temperature is known as LCST. The thermoresponsive behaviour showed by PNIPAAm originates from the interactions between its hydrophilic and hydrophobic groups – acrylamide and isopropyl groups respectively – as well as from hydrogen bonding [39]. At temperatures below the LCST, hydrogen bonds between hydrophilic segments of the polymer chain and water molecules dominate, leading to enhanced dissolution in water. This interaction makes the PNIPAAm chains to obtain a hydrated/open state, called 'coil'. However, with the increase of temperature the hydrophobic interactions between hydrophobic groups become stronger and hydrogens bonds – N-H or C=O – become weaker, which leads to the collapse of the polymer molecule [40]. After collapse, the molecule obtains a more compact/cohesive state, commonly denominated as 'globule'. The transition from an open to a more collapsed state is called 'coil-to-globule' transition [41]. This 'coil-to-globule' transition is also reflected in the behaviour of crosslinked PNIPAAm microgels. In this case, PNIPAAm microgels transit from a swollen state – related to their hydrophilic nature – to a deswollen/collapsed state. The temperature responsible for the volume change is called Volume Phase Transition Temperature (VPTT) and may or may not be the same as the LCST [42, 43].

One interesting property of PNIPAAm microgels is that its LCST, as well as the physical nature of the volume phase transition, can be modified with the addition of surfactants or salts [44] or other functional groups [45], the former being typically preformed *via* copolymerization of co-monomers into the microgel at the time of synthesis. The most commonly used co-monomer is acrylic acid (AAc). AAc is a weak acid with a pK_a of approximately 4.25, which means that at pH < pK_a the PNIPAAm microgels respond normally (transition volume phase at ~ 32ºC), while at pH > pK_a their response is hindered, thus requiring more temperature to achieve the same volume phase transition [46]. The addition of AAc to PNIPAAm microgels not only increases the LCST, but also creates new bonding sites to which further bioconjugates can be attached, turning the PNIPAAm microgels into multiresponsive structures [47, 48].

1.4 Promissing hydrogels from polyvinylpyrrolidone

Since the pioneering work of Wichterle and Lim in 1960 [49] in crosslinked Poly(2-hydroxyethyl methacrylate) (Poly-HEMA) hydrogels, these materials have been vastly explored over the years due to their hydrophilic character and biocompatibility [50-54]. Hydrogels are hydrophilic crosslinked polymer networks which can absorb water several thousand times their dry weight in water and retain their structure integrity. These polymeric networks contain covalent bonds produced by the reaction of one or more co-monomers, physical crosslinks due to chain entanglements, association bonds including hydrogen bonds or strong van der Walls interactions between chains, or crystallites bringing together two or more macromolecular chains [55, 56]. If two or more polymeric chains are held together by chain entanglements and/or secondary forces (e.g.: hydrogen bonds) the hydrogel is called 'physical' or 'reversible'. Physical gels are not homogenous since clusters of molecular entanglements, or hydrophobic domains, can give rise to inhomogeneities [57]. When the polymeric network of a hydrogel is covalently crosslinked, the hydrogel is called 'chemical' or 'permanent'. This type of hydrogel can be produced by either *in situ* monomer polymerization – which requires the presence of a bifunctional monomer – or by crosslinking the preformed macromolecule [58], making it more stable than physical hydrogels. When considering a chemical hydrogel for biomedical applications, it is preferable to produce it using a crosslinking mechanism instead of *in situ* monomer polymerization, in order to eliminate any residual monomer that could be potentially toxic.

PVP is a neutral hydrophilic water-soluble polymer with low toxicity and high biocompatibility with living tissues, capable of binding reversibly to various molecules (dyes, metals and some polymers) in solution [59, 60]. These characteristics, allied with the fact that PVP has a strong tendency to form complexes with smaller molecules, makes this polymer a strong candidate to produce drug delivery systems [61].

This polymer is very effective as a hydrogel due to the capability of incorporate water in its network when crosslinked, which is something that does not occur when PVP is in its linear form [62]. Traditionally, PVP hydrogels are obtained by either the monomer polymerization or crosslinking of the preformed polymer chains. Like any hydrogel, PVP hydrogels if synthesized *via* monomer polymerization could contain toxic residual monomers, which would need expensive and time-consuming purification [63]. Taking that in consideration, crosslinking the preformed polymer chains is more promising. In 1990 Rosiak *et al.* [64] proposed a methodology of hydrogel dressing production based on high-energy irradiation of PVP aqueous solutions, resulting in hydrogels with no potentially toxic residual monomers. The problem with this method is the use of high-radiation sources, which are very expensive and not easily available. A solution to this problem is the use of Ultraviolet (UV) radiation, not just because is cheaper than high-energy radiation, but also due to the extremely short time required for reliable gel formation [60]. During UV irradiation, the pyrrolidone substituents and cyclic amides on the PVP chains generate macroradicals – produced by UV direct photolysis of PVP – whose recombination could lead to intermolecular crosslinking PVP [65]. The results of PVP's UV direct photolysis are depicted in Figure 1.2.

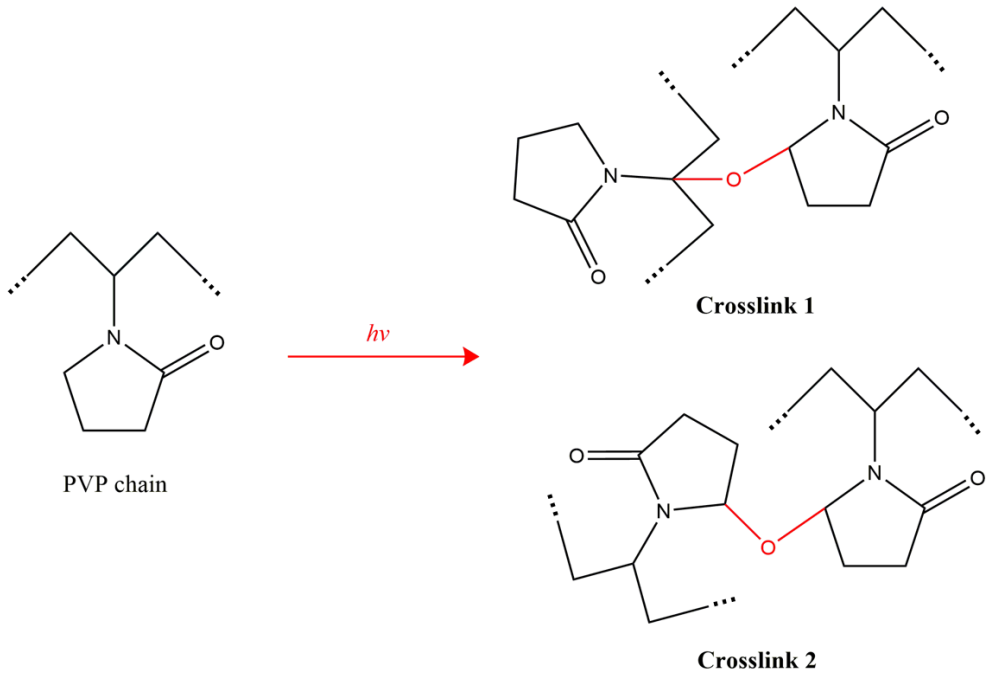

Figure 1.2 – Chemical structure of *N*-vinylpyrrolidone monomer and effect of UV irradiation on PVP chain with consequent intramolecular crosslinked PVP (adapted from [65]).

Normally hydrogels are prepared in the form of dense films, which end up being impermeable to air and liquid and have lower surface area when compared to porous materials. One way to overcome these obstacles is to create fibrous hydrogels: polymeric hydrogel meshes with high air/liquid permeability and elevated water absorbance capacity [66]. These structures, which are prepared mostly by electrospinning, are a topic of interest because of the large surface area and highly porous structure [67, 68], making them a suitable material for wound dressing [69].

In previous works done in SBM research group [3, 4], microgels and composite fibres have already been explored. Although, those works presented some drawbacks, which lead to the need to re-evaluate the used systems and further optimize them so that a stable system with various applications can be conceived. Taking into consideration the versatility of microgels and the structural stability acquired by PVP when crosslinked using UV irradiation, a composite multifunctional system can be design.

This dissertation reports on the optimization of PVP as a fibre template material. Both mechanical and swelling properties of this polymer were studied and their behaviour with different UV crosslinking times analysed. Furthermore, an attempt to confine thermosensitive PNIPAAm microgels was made, using colloidal electrospinning, in order to produce composite multifunctional systems that could be tailored for a wide range of applications.

2 Materials and Methods

2.1 Materials

N-isopropylacrylamide (NIPAAm, Aldrich Chemistry, 97%) was used as a monomer and *N,N*-methylene bis-acrylamide (MBA, Sigma-Aldrich, 99%) as crosslinker, ammonium persulfate was chosen as initiator (APS, Sigma-Aldrich, 99%) and sodium bisulphite (SBS, Acrös Organics) as catalyst. All reagents were used as received without any further purification. Acrylic acid 90% (Alfa Aesar) was used in order to study the effects in the microgels' LCST.

2.2 Synthesis of PNIPAAm microgels

PNIPAAm and PNIPAAm-AAc crosslinked microgels were synthesized by means of surfactant-free emulsion polymerization (SFEP) method. All polymerizations were conducted in a 100 mL three-necked round flask equipped with a reflux condenser, a mercury thermometer and a nitrogen inlet/outlet. The weight percentage of crosslinker, initiator and catalyst was 5%, 10% and 5% respectively. NIPAAm and MBA solutions, 50 $\mu g.mL^{-1}$ and 2.5 $\mu g.mL^{-1}$ respectively, were mechanically stirred at 400 – 500 rpm for 5 minutes and purged with nitrogen for 30 minutes. The reaction was initiated by heating the flask up to 70ºC (above PNIPAAm's LCST) with the immediate addition of the APS solution. After 1 h the catalyst solution was added. The reaction proceeded for 4 hours at constant temperature and nitrogen atmosphere. The obtained microgel dispersions were dialyzed against distilled water using a dialysis Spectra/Por molecular porous membrane (MWCO: 12 – 14,000) for a week. Finally, the microgels were freeze-dried (VaCo 2, *Zirbus*) in order to guarantee long term stability.

For the preparation of PNIPAAm-AAc microgels, different weight percentages of acrylic acid were dissolved in water, namely 6% and 10%. The acrylic acid solution was added after the NIPAAm solution and the polymerization process proceeded as previously mentioned. The quantities used to synthesize both PNIPAAm and PNIPAAm-AAc microgels, as well as the respective hydrodynamic diameters and polydispersion indexes, can be consulted in Table 6.1 and Table 6.2 respectively, available on Section 6.1 of the Supporting Information

2.3 Colloidal-electrospinning

2.3.1 Polyvinylpyrrolidone solutions

PVP solutions (Sigma-Aldrich, $\bar{M}_w$ = 1.300.000) dissolved in ethanol (Scharlau, analytical grade) were used as fibre template. The solutions were prepared by dissolving different weight percentages of PVP into ethanol (10 wt.%, and 14 wt.%) and magnetically stirred for 3 h at room temperature, to ensure complete homogenization. After that, the microgel dispersions were added into the PVP solutions in two different percentages, 5 wt.% and 10 wt.%, regarding PVP total mass. The volume of distilled water used to prepare the microgel dispersions needs to be such that the co-nonsolvency of the microgels is ensured (35:65 water:ethanol [70]), and that the microgels are confined in their swollen state.

2.3.2 Colloidal-electrospinning experiments

The electrospinning experiments were conducted using a high voltage power supply (Glassman High Voltage, EL, USA), a digitally programmed syringe pump (kdScientific) and a tin foiled cover as collector. The solutions were loaded into a 5 mL syringe fitted with a 23-gauge blunt tip needle and mounted onto a syringe pump programmed to deliver said solutions with a flow of 0.3 and 1 $mL.h^{-1}$. The process was carried out with two different applied voltages (10 and 15 kV) and two different tip-to-collector distances (TCD), namely 12 and 18 cm, in a climatic cabin with a relative humidity of 30 – 40%, in order to ensure solvent's fast evaporation, and controlled temperature, close to 25ºC, well below the microgel's LCST. Electrospinning ran for approximately 2 h and the resulting non-woven fibre mat was dried for 24 h, in order to remove any remaining solvent.

As for the colloidal electrospinning, the parameters used result from the electrospinning optimization study: 14 wt.% PVP/EtOH polymeric solution, 15 kV of applied voltage, 12 cm TCD, relative humidity between 30 – 40% and temperatures ranging from 20 – 25ºC. The flow rate used was 0.7 $mL.h^{-1}$, which is lower than the optimized (1 $mL.h^{-1}$). This change will be further discussed in the Results and Discussion Section.

2.4 PVP film preparation

A solution of 40 wt.% of PVP in ethanol was shear cast into several films using an Automatic Film Applicator (Braive Instruments) fitted with a 1 mm adjustable Filmographe baker with a shear rate of 1.25 $mm.min^{-1}$. The thin films were dried for 48 h in order to fully evaporate the solvent.

2.5 UV crosslinking method

PVP thin films, membranes and composite membranes were crosslinked with 254 nm ultraviolet light in a *BIO-LINK*® irradiation system. The films were irradiated for 1, 2, 3 and 5 h, while the membranes were irradiated for 5, 10, 15, 20, 30, 40 and 60 minutes.

2.6 Characterization techniques

Scanning electron microscopy (SEM) technique was used in order to evaluate the morphology of the obtained fibres. For the electrospinning optimization study, the samples were prepared with a gold coating and analysed using a Zeiss DSM 962 scanning electron microscope. As for the membranes that were produced after the optimization study, their morphology was studied using a SEM apparatus fitted with a Carl Zeiss Auriga CrossBeam system (SEM-FIB). A small piece of fibre mat was fixed on carbon tape and then mounted on a support and sputtered with a thin layer of gold/palladium using a Q300T D Quorum sputter coater. The diameter and distribution of the overall electrospun fibres were determined using ImageJ software.

Dynamic light scattering (DLS) technique was used to determine the microgels' hydrodynamic diameter and to study their behaviour at different temperatures. The equipment used is a Horiba Nanopartica Analyzer SZ-100 equipped with a 594 nm He-Ne laser and a Peltier element to control the temperature. All measurements were carried out for diluted suspensions (1 $mg.mL^{-1}$) at a temperature range from 22 – 46ºC in disposable cuvettes.

Tensile tests were performed in order to study the non-woven mats and film's mechanical response. Non-woven mats, films and colloidal membranes' samples were cut into 10x5 mm rectangles and mounted onto a pair of clamps and stretched at a speed of 0.1 $mm.min^{-1}$.

Fourier transform infrared (FTIR) transmission was used to study the chemical composition of the crosslinked membranes. The equipment used was a FTIR Thermo Nicolet 6700 spectrometer with the transmission spectra being collected at room temperature, from 4500 to 500 cm^{-1}, using an attenuated total reflectance (ATR) accessory equipped with a single-bounce diamond crystal with an incident angle of 45º.

3 Results and Discussion

3.1 Polyvinylpyrrolidone membranes

The focus of this dissertation is the optimization of the polymeric matrix, PVP, in order to obtain fibres with a monodisperse distribution of diameters as well as a minimum mean fibre diameter. To do so, a study where electrospinning parameters such as polymer solution concentration, process flow rate, applied voltage and tip-to-collector distance (TCD) were varied in specific ranges was performed. For this electrospinning process, temperature was kept between 20 – 25ºC and the RH between 30 – 40%, since these are the ranges that guarantee the formation of PVP fibres [71].

3.1.1 Optimization of electrospinning process

Like previously stated, the diameter of the polymeric fibres can be influenced by several parameters, which are normally gathered into three groups: i) solution parameters, ii) process parameters and iii) environmental conditions. For instance, both polymer's concentration and process flow rate influence the fibre's diameter in the same manner: with the decrease of concentration/flow rate, thinner fibres can be obtained [72]. As for the applied voltage, fibres with smaller diameters can be obtained when working with stronger electric fields. However, when working with high electric field the probability of beads formation is higher [73]. Another parameter of great influence in the electrospinning process is relative humidity (RH), which affects the solvent's evaporation and thus the formation of pores on the fibre surface. De Vrieze *et al* studied the effect of temperature and humidity on PVP fibres and concluded that, at higher RH the absorption of the surrounding water causes slower solidification, longer jet elongation time and therefore lower fibre diameters [71]. However, over 60% RH, the fibres start to fuse with each other, resulting in larger diameters.

3.1.1.1 Influence of polymer concentration

Two different solutions of PVP dissolved in ethanol – 10 and 14 wt.% – were prepared and electrospun. For this part of the study, the flow rate, applied voltage and tip-to-collector distance constant were constant – 0.3 $mL.h^{-1}$, 15 kV and 18 cm respectively – in order to see just the effect of the solution's concentration. The resulting fibres and respective mean fibre diameters (MFD) are depicted in Figure 3.1. The MFD for all the parameters' variations can be consulted in Table 6.3, available at Section 6.2 of the Supporting Information.

As it can be seen from Figure 3.1, there is an increase of MFD with the increase of the solution's concentration: MFD of 585 ± 64 nm for a 10 wt.% PVP/EtOH solution to a MFD of 710 ± 97 nm for a 14 wt.% PVP/EtOH solution. The polymer concentration influences both the viscosity and surface tension of the solution, two parameters that are very important in the electrospinning process. On one hand, if the solution is too dilute – low viscosity – the dominant factor is the surface tension of the droplet, which results in the inability of forming a continuous fibre and mainly drops of solution or beaded fibres will reach the collector. On the other hand, if the solution is highly viscous, the electric field may not be high enough to disrupt the viscoelastic forces , which can lead to the formation of fibres with several different diameters [74]. Thus, there is an optimal range of polymer concentration for which polymer chain entanglements are enough, condition required for the formation of fibres. Newsome *et al.* reported the successful

electrospinning of silica/PVP (SiO_2/PVP) composite nanofibers, where PVP fibres were obtained using 9, 10 and 11 wt.% PVP solutions, with the 11 wt.% PVP solution originating the nanofibres with the highest diameter [75].

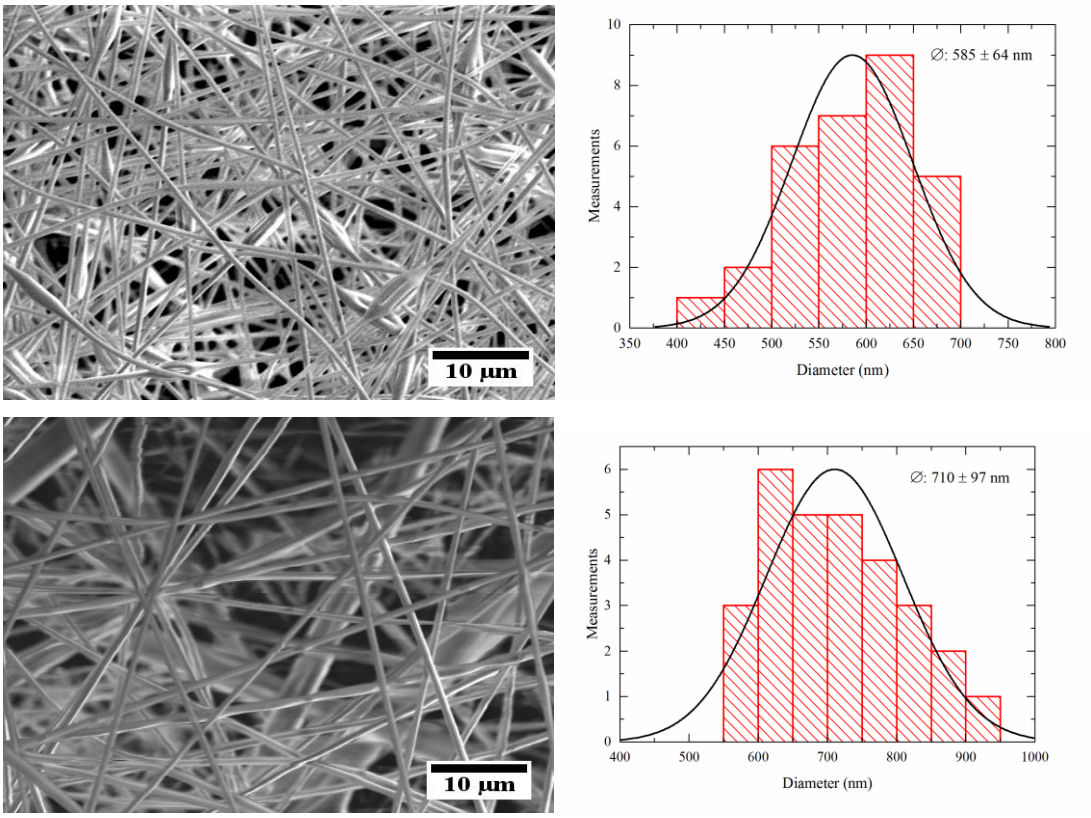

Figure 3.1 – SEM micrographs of PVP non-woven mats, and respective MFD, electrospun from 10 wt.% (top) and 14 wt.% (bottom) PVP/EtOH solutions. The electrospinning process was conducted using a 0.3 $mL.h^{-1}$ flow rate, 15 kV and 18 cm TCD. All scale bars represent 10 µm.

Nevertheless, the solution with a concentration of 10 wt.% formed fibres with beads (which was not desired). The remaining influencing factors (flow rate, applied voltage and TCD) in this optimization were all performed using the 14 wt.% solution, which did not present any sort of defects, although the mean fibre diameter of the fibres is higher (Figure 3.1)

3.1.1.2 Influence of process flow rate

In this case, two different process flow rates where studied – 0.3 and 1 $mL.h^{-1}$ – while the polymer concentration, the applied voltage and the TCD were kept constant at 14 wt.%, 10 kV and 12 cm respectively.

The process flow rate not only affects the fibre diameter but also its porosity and shape. The effect of this parameter is the same as the polymer concentration one: with the increase of flow rate there is an increase in the fibre's diameter. Since the flow rate determines how much solution is available at the tip of the needle for fibre formation, for a given voltage there is a lower limit of flow rate for the Taylor cone to be stabilized [75]. If the flow rate is increased above this limit the fibre diameter increases because there is a greater volume of solution at the tip than the one that can be ejected. Another consequence of a high process flow rate is the formation of significant amounts of beads, each resulting from the incomplete drying process of the fibres before reaching the collector [74]. Figure 3.2 shows the obtained fibres for each process flow rate tested.

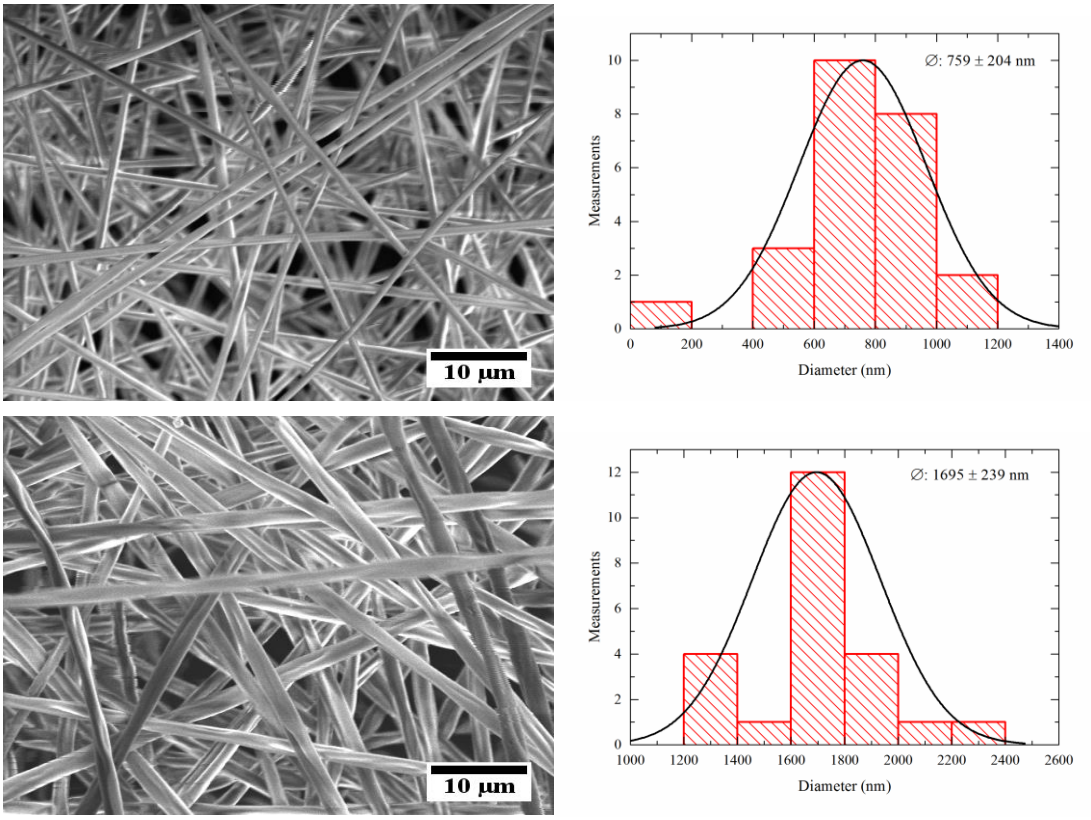

Figure 3.2 – SEM micrographs of PVP non-woven mats, and respective MFD, electrospun from a 14 wt.% PVP/EtOH solution with a flow rate of 0.3 mL.h^{-1} (top) and 1 mL.h^{-1} (bottom). The electrospinning process was conducted using 10 kV and 12 cm TCD. All scale bars represent 10 µm.

As it was expected, MFD increases with the increasing flow rate (759 ± 204 nm for 0.3 mL.h^{-1} to 1695 ± 239 nm for 1 mL.h^{-1}). Since both flow rates enabled the production of electrospun fibres, it can be said that the lower limit at which the Taylor cone can be stabilized was not exceeded. Consequently, depending on the desired MFD, both flow rates can be used to successfully produce PVP electrospun fibres.

3.1.1.3 Influence of applied voltage

In order to study the influence of the applied voltage on the fibre's diameter, 10 and 15 kV were applied to the tip of the needle during the electrospinning process. Once again, all the other parameters remained constant; in this case, the chosen polymer concentration was 14 wt.%, the flow rate 1 mL.h^{-1} and the TCD was 12 cm. Figure 3.3 shows the results for the variation of the applied voltage.

When high voltages are applied, the polymer jet suffers a greater stretching due to the greater columbic forces and stronger electric field, which leads to thinner fibres. However, applying lower voltages results in the reduction of the polymer jet's acceleration, which increases its time of flight and consequently its stretching ability [76].

In this study it is possible to observe (Figure 3.3) that with an increase of the applied voltage there is a decrease in the MFD (759 ± 205 nm for 10 kV and 710 ± 97 nm for 15 kV). Nevertheless, the applied voltage did not affect the fibres MFD, in the tested range.

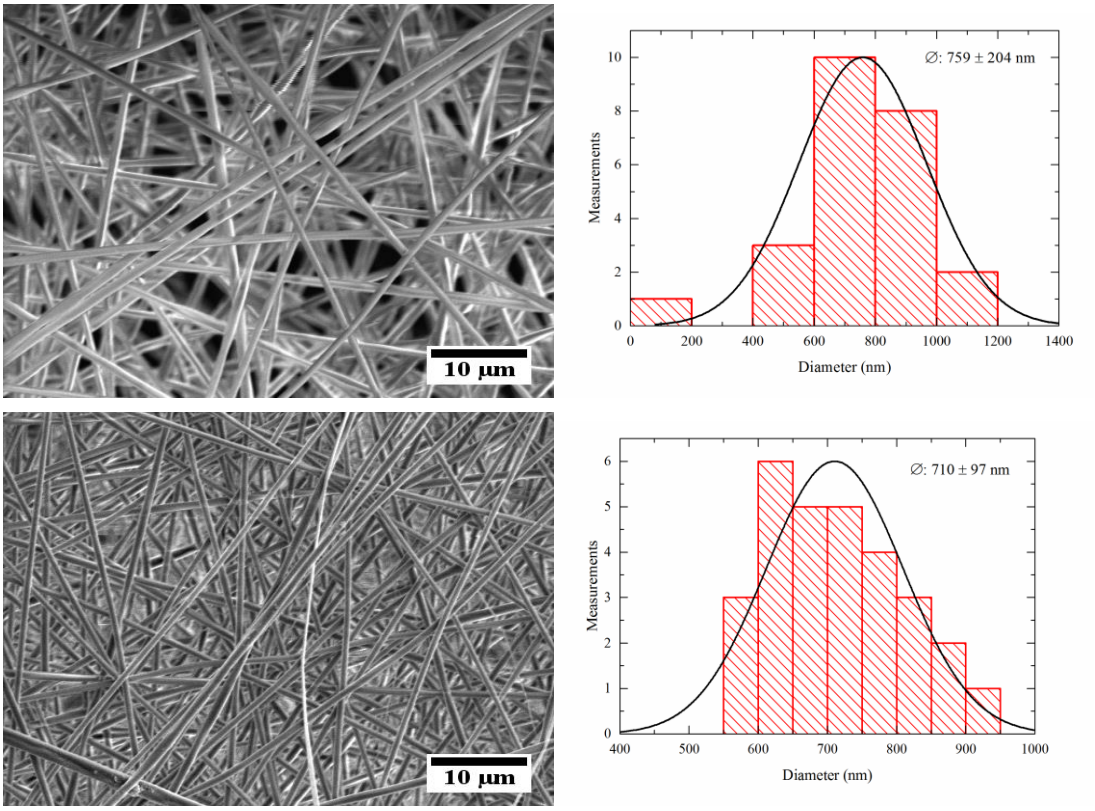

Figure 3.3 – SEM micrographs of PVP non-woven mats, and respective MFD, electrospun from a 14 wt.% PVP/EtOH solution with an applied voltage of 10 kV (top) and 15 kV (bottom). The electrospinning process was conducted using a flow rate of 0,3 $mL.h^{-1}$ and 12 cm TCD. All scale bars represent 10 µm.

3.1.1.4 Influence of tip-to-collector distance

The variation of the tip-to-collector distance mainly affects the fibre's time of flight, which consequently influences the solvent's evaporation. If the flight time is not enough, there will be an incomplete evaporation of the solvent that will lead to the formation of fused fibres [75]. As for the MFD it usually increases with the increasing TCD, although it has been reported that it is possible to obtain thinner fibres with higher TCD [76].

The TCD has a great influence on the area of the collected fibre mat which can vary depending on the application in mind. During the electrospinning process, the fibre jet that is accelerated from the polymer droplet starts in a straight line-like shape and progressively begins to bend, in order to reduce the density of surface charge, to promote jet extension and increase surface area. This 'unstable whipping' creates a cone perpendicular to the collector's plane, forcing the deposited fibre mats to take a circular shape (base of the cone) [75]. Depending on the TCD, and maintaining the polymer concentration, applied voltage, flow rate and deposition time constants, one can obtain thinner or thicker fibre mats, using lower or higher TCD respectively.

In this work 12 and 18 cm TCD were tested, with the results being showed in Figure 3.4. The fibres in SEM micrographs were electrospun from a 14 wt.% PVP/EtOH solution using a flow rate of 1 $mL.h^{-1}$ and 15 kV of applied voltage.

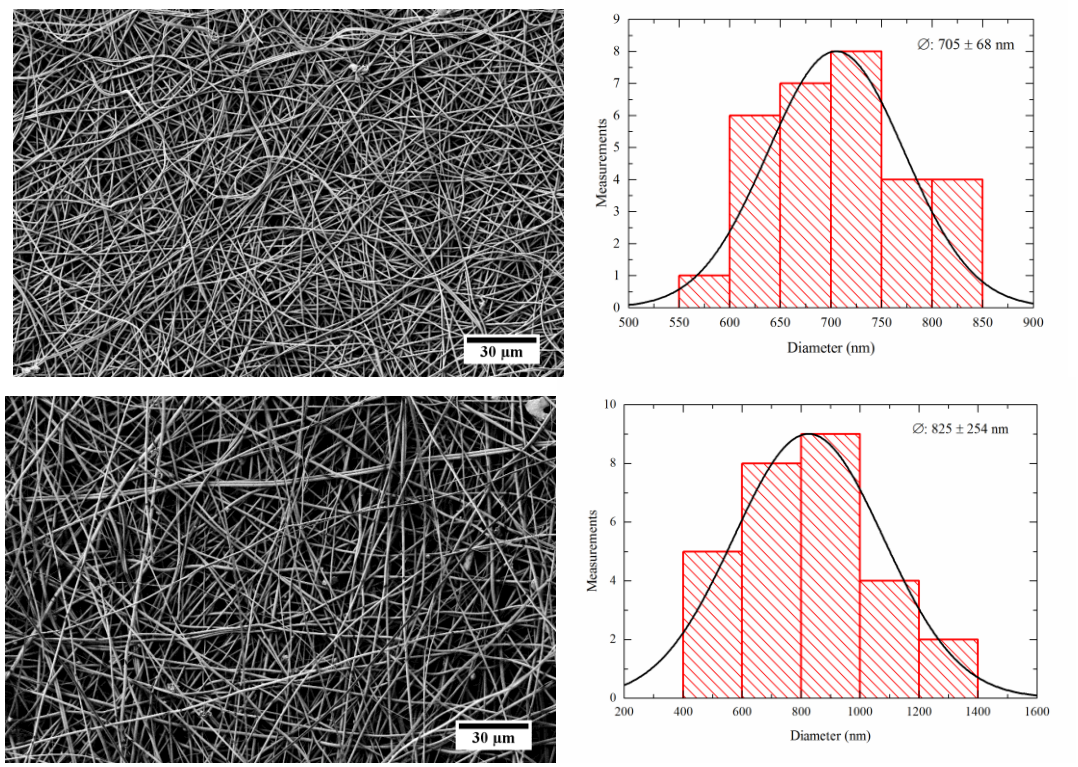

Figure 3.4 – SEM micrographs of PVP non-woven mats, and respective MFD, electrospun from a 14 wt.% PVP/EtOH solution with a TCD of 12 cm (top) and 18 cm (bottom). The electrospinning process was conducted using a flow rate of 1 mL.h^{-1} and 15 kV.

After studying the influence of the target-to-collector distance, a small increase in MFD was observed with the increase of TCD (705 ± 68 nm for 12 cm TCD and 825 ± 254 nm for 18 cm TCD). The non-woven mat produced with 12 cm TCD appears to be denser than the 18 cm TCD one. Since the 12 cm one is closer to the tip of the cone (confirmed by the unstable whipping of the accelerated jet), and since both mats were electrospun for 15 minutes, for the same amount of time the collector that was closer to the cone tip enable the deposition of a denser non-woven mat. Moreover, the electrospun non-woven mats produced using a TCD of 18 cm have a wider dispersion of diameters, from 400 nm to 1400 nm. Therefore, the TCD of 12 cm is more appropriate for the desired optimization. Like it was previously said, the study that was made to obtain the more monodispersed distribution of fibres was conducted by varying all the parameters, although not all combinations are presented in this chapter. Table 6.3 on Section 6.2 of the Supporting Information contains all the MFD resulting from this study.

After the optimization process, the most suitable parameters were determined to be a 14 wt.% PVP/EtOH solution, flow rate of 0.3 and 1 mL.h^{-1}, 10 or 15 kV of applied voltage, 12 cm TCD, a RH range of 30 – 40% and process temperature between 20 to 25ºC.

3.2 Process-dependent comparative study: non-woven mats *vs.* films

The main difficulty that these non-woven mats present is the lack of structural stability when submerged in water, since PVP is water soluble. In order to overcome the said obstacle, the chosen approach consisted in crosslinking the PVP matrix. There are several options to crosslink PVP, from high-energy irradiation [64] to temperature treatments [66]. Although high-energy irradiation treatments have been proved to crosslink PVP with no potentially

toxic residual monomers, they are expensive and not easily available. In this dissertation PVP was crosslinked by means of UV irradiation, a green and cost-effective technique that allows the increase of the system's structure stability. To do so, the non-woven mats, cut into 10x5 mm samples, were placed inside a *BIO-LINK*® crosslinker and irradiate at 254 nm, which is found within the PVP absorption spectrum (200 – 280 nm). When exposed to this range of radiations, pyrrolidone substituents and cyclic amides on the PVP chains generate macroradicals whose recombination leads to intermolecular crosslinked PVP. The achieved crosslinking degree will depend in the irradiation dose and hence in the time that the non-woven mats are irradiated.

Therefore, in order to determine the most suitable conditions (irradiation time) to crosslink the PVP non-woven mats, and to better understand the behaviour of UV crosslinked PVP, a process-dependent comparative study was conducted: non-woven mats vs. films. For the comparative study, PVP films were prepared from a 40 wt.% PVP/EtOH solution by shear casting method (v = 1.25 $mm.min^{-1}$) and left to dry for 48 h to guarantee complete solvent evaporation. The non-woven mats were irradiated for 5, 10, 15, 20, 30, 40 and 60 minutes, whereas the shear-casted PVP films were irradiated for 1, 2, 3 and 5 h. The difference between the irradiation time of the non-woven mats and the films can be explained by the high surface area to volume ratio of the mats: a higher ratio means more area available to be crosslinked, hence less irradiated time is required to achieve the same goal.

3.2.1 UV crosslinking influence in morphology

In order to study the influence of UV irradiation in morphology, SEM micrographs were taken for both non-woven mats and films. Figure 3.5 and Figure 3.6 depict the evolution of the non-woven mats and films morphologies with increasing irradiation time.

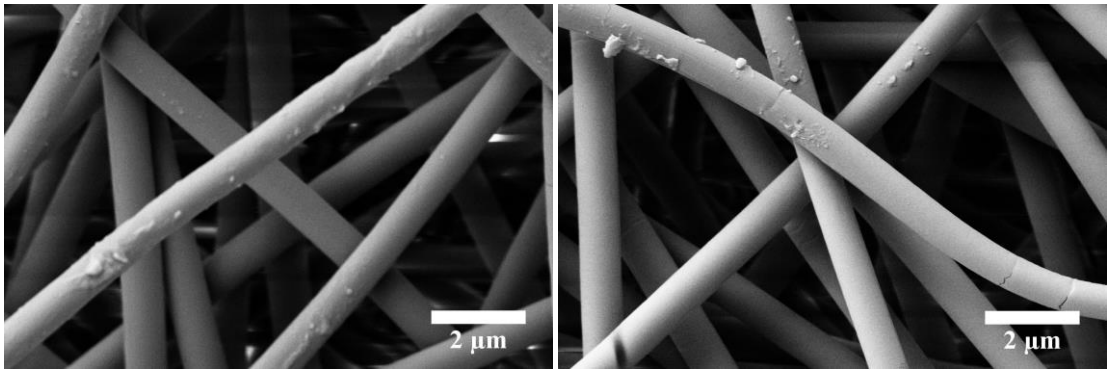

Figure 3.5 – SEM micrographs of PVP fibres crosslinked for 5 minutes (left) and for 60 minutes (right) under UV radiation. The micrographs were obtained using a 10k x magnification, a 5 kV electron beam, an aperture size of 30 µm and a WD of 5.8 mm.

For the non-woven mats morphology (Figure 3.5), there are no great changes in the MFD with the increase of irradiation time, since all non-woven mats have a MFD of approximately 830 nm (for full data the reader can consult Table 6.4 in Section 6.3 of the Supporting Information). However, with 60 minutes of UV irradiation there are some visible cracks on the fibres' surface, possibly indicating excessive irradiation time.

Regarding the films morphology, it is visible that with 1 h of UV irradiation the film presents wrinkles, indicating that it has possibly absorbed water from the surrounding environment [59] (Figure 3.6, left micrograph). This is an indicator that 1 h of irradiation may not be enough to fully crosslink the polymer network. As for the 5 h irradiated film, there

are cracks throughout the entire film's surface (Figure 3.6, right micrograph), which may be an indicator of excessive irradiation time.

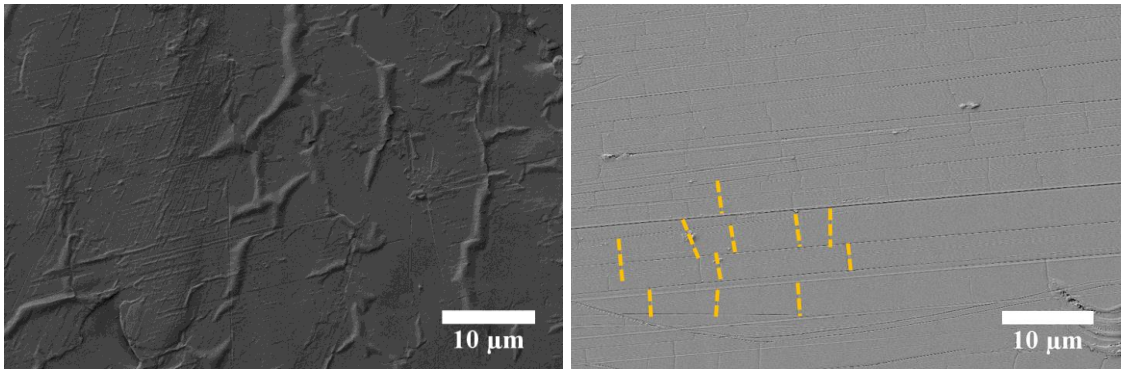

Figure 3.6 – SEM micrographs of PVP films crosslinked for 1h (left) and 5 h (right) under UV radiation. The micrographs were obtained using a 2k x magnification, a 2 kV electron beam, an aperture size of 30 µm and a WD of 5.6 mm.

In order to better understand the influence of the UV irradiation treatment, an indirect evaluation of the crosslinking method was performed by studying the mechanical properties of both non-woven mats and films, as well as their swelling properties.

3.2.2 UV crosslinking influence in the mechanical properties

PVP films – with a mean thickness 22 ± 3 µm – were treated with different UV exposure times, (1, 2 and 5 h). For each irradiation time samples cut on the parallel and perpendicular directions to the shear cast direction were tested, being the results for Young's Modulus (*E*), Ultimate Tensile Strength (UTS) and Elongation at break (ε) presented in Table 6.5 available on Section 6.4 of the Supporting Information.

When a film is shear-casted, the polymer chains get aligned in the direction of the shear vector, which results in a polymeric film where polymer molecules have a preferential orientation. This preferential orientation may have some influence on the film's mechanical properties. To infer on the effects of said preferential orientation, the PVP films' mechanical properties were studied using samples cut in both the parallel and perpendicular directions to the shear vector. After the assessment of the mechanical properties, it was found that there are no great differences between the samples stretched in the parallel and perpendicular to the shear direction (Table 6.5, Section 6.4 at Supporting Information). Figure 3.7 shows two representative curves of the performed mechanical tests.

Concerning the irradiation time, it was macroscopically observed that above 5 h of irradiation the films turned yellow, which indicates that PVP has suffered photodegradation [59]. Therefore, three different times were studied, namely 1, 2 and 5 h. One of the effects that photodegradation has in PVP is the increase of the elongation at break. If a polymer is irradiated for long periods of time it suffers photodegradation, which leads to the formation of small molecular groups that act as plasticisers [77]. These plasticisers are responsible for the increase of elongation (0.67 ± 0.14% for 1 h UV irradiation to 2.0 ± 0.37% for 2 h UV irradiation) as it is shown in Table 6.5. Although, when passing from 2 h to 5 h irradiation time, the elongation at break decreases, possibly due to oxidation, destruction of the crystal regions or the formation of new order range [77].

To comprehend the differences of the polymer matrix – non-woven mats and films – both the evolution of the Young's Modulus and the UTS with the irradiation time were plotted, like it is shown in Figure 3.8.

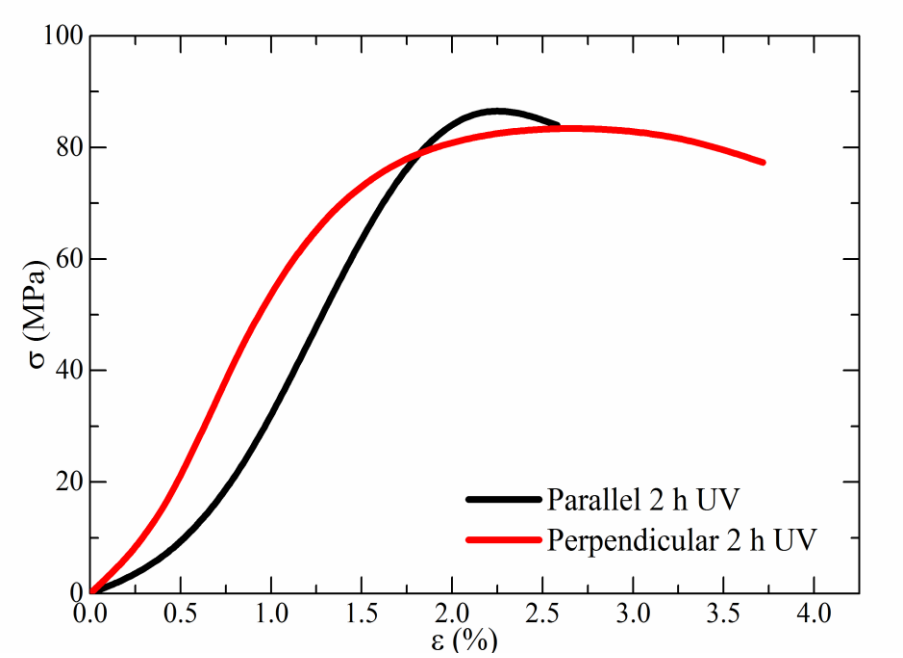

Figure 3.7 – Stress/Strain curves for PVP films with 2 h UV irradiation in parallel and perpendicular directions to the shear. Similar results were obtained for all irradiation times.

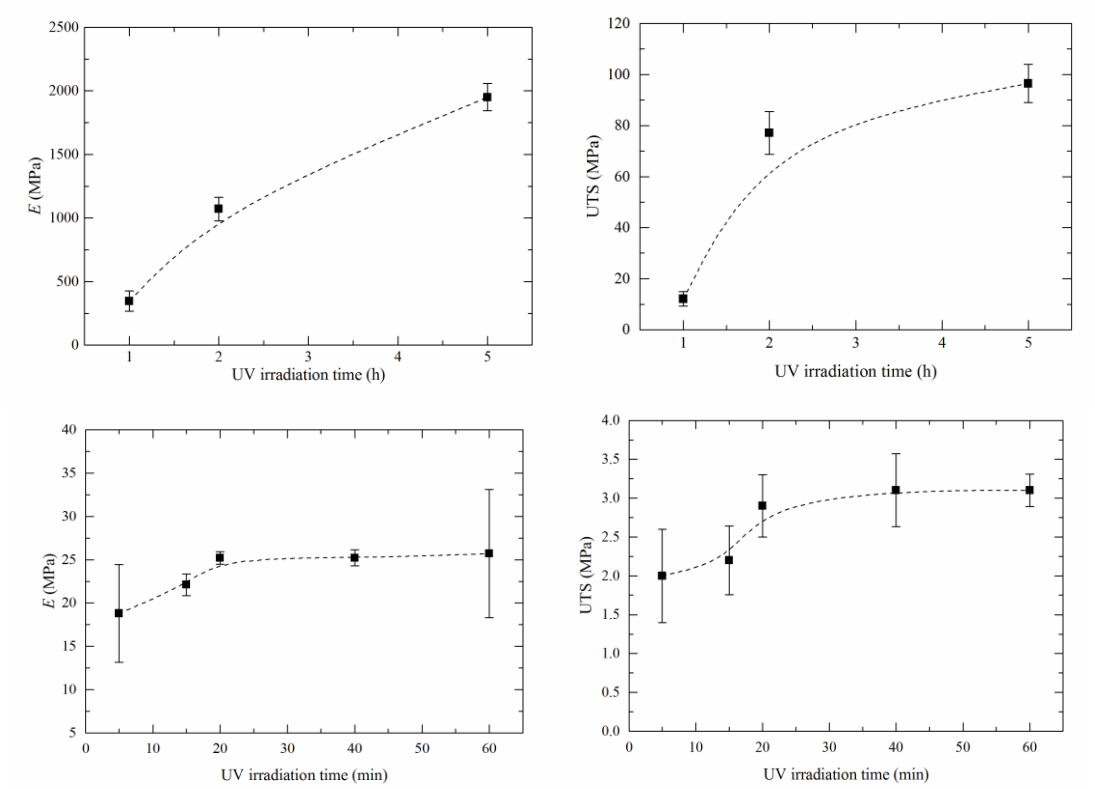

Figure 3.8 – Evolution of Young's Modulus and UTS with increasing irradiation time for PVP films (top row) and PVP non-woven mats (bottom row).

By analysing the plots in Figure 3.8 it is possible to say that, for the irradiation times studied, the polymeric matrix shows different mechanical behaviours for the different preparation techniques (shear casting vs. electrospinning). Regarding the films behaviour (Figure 3.8, top row) both Young's Modulus and UTS increase with increasing irradiation times (Table 6.6 on Section 6.4 of the Supporting Information). This increase could be related to an increase of crosslinking degree, but further studies with intermediary and higher irradiation times should be performed in order to better assess this behaviour. As for the non-woven mats (Figure 3.8, bottom row), an equilibrium for the Young's Modulus and the UTS is reached after 20 minutes of irradiation time, which means that irradiating the mats for more than 20 minutes does not bring a visible advantage to the system's mechanical properties. Although the mechanical properties do not change, the morphology is in fact affected with the increase of irradiation time (appearance of cracks for 60 minutes of UV irradiation time).

3.2.3 UV crosslinking influence in the swelling properties

In order to study the influence of the UV irradiation time in the crosslinking process of the PVP films, their swelling properties were evaluated. For that, 6 rectangular samples (10x5 mm) of each irradiated film – 3 in the parallel and 3 in the perpendicular directions of the shear – were immersed in water for 0.5, 1, 2, 3 and 5 h. Between each immersion time the water was changed in order to eliminate any possible non-crosslinked polymer chains resulting from the dissolution. Swelling ratio curves were plotted to see when the samples would reach an equilibrium state with the surrounding medium (Figure 3.9).

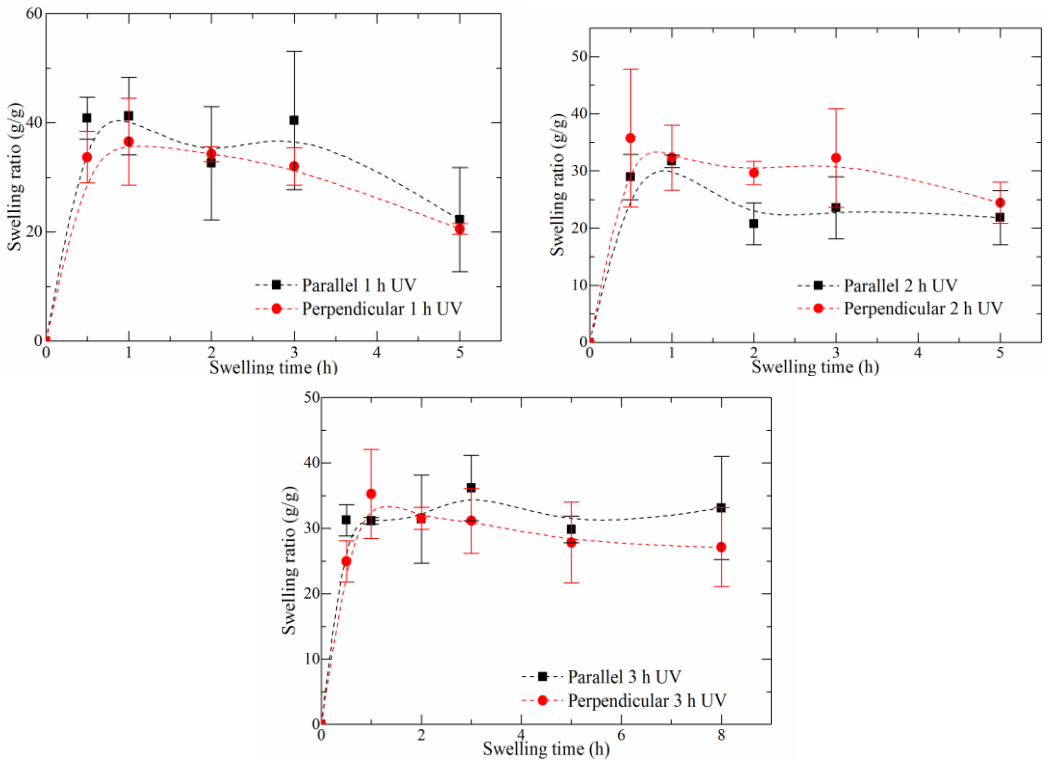

Figure 3.9 – Swelling ratio curves for UV crosslinked PVP films with an irradiation period of 1 h (top left), 2 h (top right) and 3 h (bottom middle).

The swelling ratio (Q) for each point in the curves was obtained using Eq. (3.1)

$$Q = \frac{w_s - w_d}{w_d} \tag{3.1}$$

where w_s is the weight of the film after immersion and w_d the weight of the film prior to immersion.

By analysing the swelling ratio curves plotted in Figure 3.9, it is observed that all the samples reached their maximum swelling capability at around 1 h, which from now on will be referred to as t_{swell}. The variation of the irradiation time did not cause significant differences between samples of the same group – samples with same irradiation time but different shear direction alignment. For instance, the sample with 2 h of irradiation has maximum swelling ratio values of approximately 31 and 32 (parallel and perpendicular alignment to shear direction, respectively).

The UV crosslinking process effect on the polymer's network can also be studied using the swelling ratio curves. Regarding the 1 h irradiated film, the film's swelling capability starts to slowly decrease after t_{swell}, which may indicate that the polymer is being dissolved (Figure 3.9, top left). This gradual decrease leads to the conclusion that 1 h of UV irradiation may not be enough to fully crosslink the PVP films, allowing the dissolution of the polymer as reflected in the decrease of swelling ratio. The 2 h irradiated film has a different behaviour than the 1 h one: after t_{swell}, the 2 h film has a small decrease in swelling capability, followed by a stable period that last for approximately 3 hours. This stable period indicates that the film reached equilibrium with its surrounding medium, meaning that no more water is neither penetrating nor leaving the polymer's network. Approximately 3 h after t_{swell} is observed, a small decrease in swelling capability occurs, indicating once again the polymer's possible dissolution (Figure 3.9, top right). As for the 3 h irradiated film, it presents a higher equilibrium period (up to 5 h), which indicates that out of the three irradiation times tested, this was the one that was able to better crosslink the PVP films.

From the analysis of the swelling properties it is possible to calculate the network mesh size, which is directly related to the crosslinking degree of the polymer network after UV crosslinking process by the application of the Equilibrium Swelling theory [78]. When studying a hydrogel's behaviour in a liquid medium there are three parameters that stand out for the characterisation of the network structure: i) polymer volume fraction in the swollen state ($v_{2,s}$), ii) molecular weight of the polymer chain between two neighbouring crosslinking nodes (M_c) and iii) mesh size (ξ). The polymer volume fraction in the swollen state is a measure of the amount of fluid that the hydrogel's network can absorb and retain. The molecular weight between two neighbouring crosslinking nodes measures the degree of crosslinking of the polymer, whether is chemical or physical crosslinking. Lastly, the mesh size gives information about the available space for fluid diffusion between the macromolecular chains. Both M_c and mesh size can only be average values due to the fact that the crosslinking process is completely random [55]. These three parameters are related to one another and can be determined with the help of the Equilibrium swelling theory.

The Equilibrium Swelling theory, first proposed by Paul Flory and John Rehner [78], states that a crosslinked polymer gel, when immersed in a fluid and allowed to reach equilibrium with its surroundings, is subject only to two opposing forces: the thermodynamic force of mixing and the retractive force of the polymer chains. When factoring the influence of these two forces, the molecular weight between two neighbouring crosslinking nodes of a neutral hydrogel prepared in the absence of a solvent can be calculated, like is showed in Eq. (3.2).

$$\frac{1}{\overline{M}_c} = \frac{2}{\overline{M}_n} - \frac{\left(\bar{\upsilon}/V_1\right)\left[\ln\left(1-\upsilon_{2,s}\right)+\upsilon_{2,s}+\chi_1\upsilon_{2,s}^2\right]}{\upsilon_{2,s}^{1/3}-\frac{\upsilon_{2,s}}{2}} \tag{3.2}$$

Here, $\overline{M}_n$ is the molecular weight of the polymer chains prepared without a crosslinker, $\bar{v}$ is the specific volume of the polymer, V_1 is the molar volume of water (18 $cm^3.mol^{-1}$) and χ_1 is the Flory interaction parameter. This equation however cannot be applied to hydrogels prepared in the presence of water. For that, Peppas and Merril modified the original Flory-Rehner theory in order to consider the volume fraction of the chains in the relaxed state ($v_{2,r}$), i.e. immediately after crosslinking [55]. Eq. (3.3) shows the modifications to the Flory-Rehner equation.

$$\frac{1}{\overline{M}_c} = \frac{2}{\overline{M}_n} - \frac{\left(\bar{\upsilon}/V_1\right)\left[\ln\left(1-\upsilon_{2,s}\right)+\upsilon_{2,s}+\chi_1\upsilon_{2,s}^2\right]}{\upsilon_{2,s}\left[\left(\frac{\upsilon_{2,s}}{\upsilon_{2,\mathrm{r}}}\right)^{1/3}-\left(\frac{\upsilon_{2,s}}{2\upsilon_{2,\mathrm{r}}}\right)\right]} \tag{3.3}$$

Before calculating the value of $\overline{M}_c$, it is required to determine the polymer volume fraction in the swollen state ($v_{2,s}$). This can be achieved by dividing the weight of the polymer in the dry state for the weight in the swollen state. The results for $v_{2,s}$ and $\overline{M}_c$ of all samples can be consulted in Table 6.7, Table 6.8 and Table 6.9 available on Section 6.5 of the Supporting Information.

Using Eq. (3.3), and knowing that PVP specific volume (v) is 0.785 $cm^3.g^{-1}$ [58], the Flory interaction parameter for PVP is 0.48 and the molar volume of water is 18 $cm^3.mol^{-1}$, the molecular weight of the polymer chain between two neighbouring crosslinking nodes can be determined [62]. This parameter is especially important because it influences both the polymer's mesh size and the crosslinking density ρ_x, which can be calculated using Eq. (3.4) and (3.5) respectively.

$$\xi = \upsilon_{2,s}^{-1/3}\left(\frac{2C_n\overline{M}_c}{M_r}\right)^{1/2}\times l \tag{3.4}$$

$$\rho_x = \frac{1}{\upsilon\overline{M}_c} \tag{3.5}$$

In Eq. (3.4) C_n is the Flory characteristic ratio, l is the length of the bond along the polymer's backbone and M_r the molecular weight of the repeating units from which the polymer chain is composed. Since the polymer used in this work was PVP, the values for C_n, M_r and l are 12.3, 111.14 $g.mol^{-1}$ and 1.54 Å respectively [62]. The mesh size and crosslinking density values are presented in Table 6.10 and Table 6.11 on Section 6.5 of the Supporting Information, respectively.

In order to study the influence of the UV irradiation time on the films' mesh size and crosslinking density, the evolution of said parameters with the increasing UV irradiation time for a fixed swelling time (5 h) was plotted as Figure 3.10 shows.

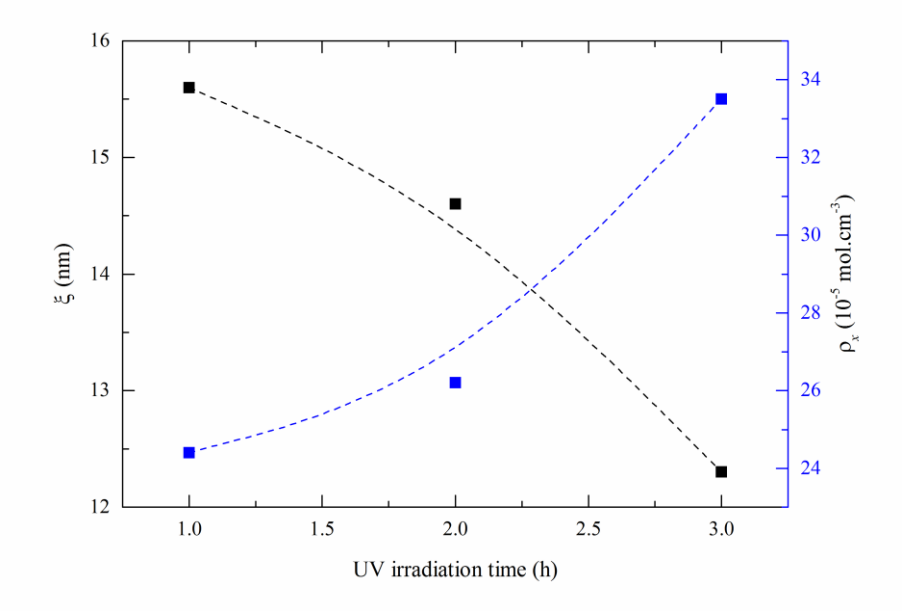

Figure 3.10 – Evolution of PVP films' mesh size (black line) and crosslinking density (blue line) with increasing UV irradiation time, considering a swelling time of 5 h.

By analysing the simultaneous variation of the mesh size and crosslinking density depicted in Figure 3.10 it can be seen that these parameters are inversely proportional. This is expected since higher irradiation periods lead to higher crosslinked films, i.e. a film with a lower irradiation period has a less dense network than one with a higher irradiation period, which means that at a certain period of time equal for both films (in this case, 5 h of immersion), the one that is less crosslinked presents a higher mesh size.

In the previous section, it was observed that films with higher irradiation times present higher values of Young's Modulus and UTS. Considering the swelling properties results, some new conclusions can be drawn. Films with higher irradiation times present a higher crosslinking density, i.e. a denser network. With a denser network, the applied force required to rupture a film, as well as the force that is applied per unit of area, is higher, which means that films with higher irradiation times should present higher UTS and Young's Modulus. This increase is in fact visible and can be consulted on Table 6.5 over at Section 6.4 of the Supporting Information. This however does not discard the fact that more irradiation times should be studied.

In the same way that it was done for the PVP films, three samples of PVP non-woven mats with different irradiation times were immersed in water to study their swelling behaviour. The chosen samples were the ones that undergone irradiation times of 5, 30 and 60 minutes, with the respective results being presented on the left graph of Figure 3.11.

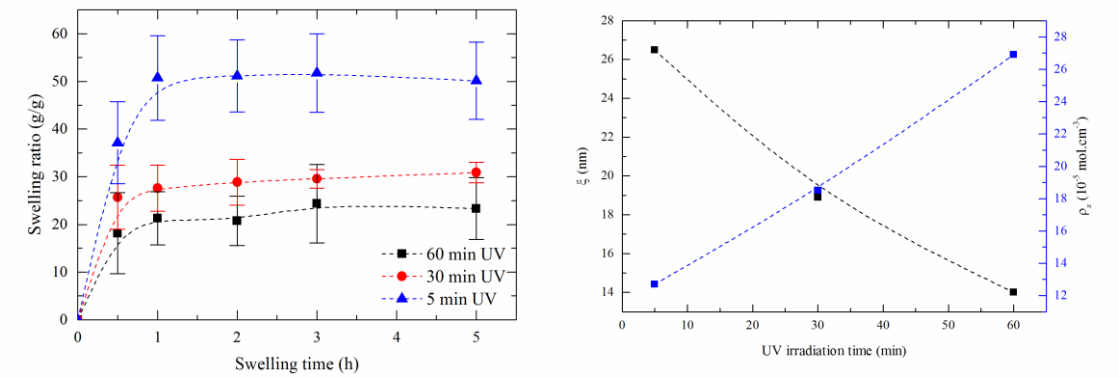

Figure 3.11 – (Left) Swelling ratio curves for UV crosslinked membranes with an irradiation period of 5 minutes (triangle), 30 minutes (circle) and 60 minutes (square). (Right) Variation of the membranes mesh size (black line) and crosslinking density (blue line) with increasing UV irradiation times.

By looking at the swelling ratio curves plotted on the left graph of Figure 3.11, a big difference between the non-woven mats that were irradiate for 5 minutes and the ones that were irradiate for 30 minutes stands out. This could be explained using the crosslinking density data, calculated from the swelling ratio and plotted on the right graphic of Figure 3.11 (for full mesh size and crosslinking density data consult Table 6.13 available at Section 6.6 from the Supporting Information). When a non-woven mat or film is crosslinked, a polymeric network is formed. In our case, with an increase of irradiation time there is an increase in the crosslinking density of the formed network. At the same time that the network gets denser its polymeric chains suffer a decrease in mobility, which ultimately results in a lower uptake of water, thus making the non-woven mats that were irradiated for 5 minutes have a higher swelling ratio than the ones that were irradiated for 30 minutes. As for the difference in swelling ratio between the 30 and 60 minutes irradiated membranes, it can be considered as negligible. This slight difference can also indicate that the ideal irradiation time may be 30 minutes, considering both the results from the mechanical properties and the morphology study. When comparing the swelling properties of the non-woven mats with the ones from the films, it is observed that non-woven mats swell almost as much as films. This can be related to the high surface to volume ratio and porosity presented by the electrospun non-woven mats.

After electrospinning process optimization and the comparative study (non-woven mats vs. films), an attempt to confine microgels into PVP non-woven mats using colloidal electrospinning technique was made. To do so, microgels dispersions were firstly studied and then confined into the PVP non-woven mats.

3.3 Composite membranes

The objective of the present work is the development of composite fibres able to form membranes with potential to tune its surface wettability. Up to this point it was confirmed that it is possible to obtain crosslinked PVP fibres able to swell (and not dissolve) in water. In order to transform PVP membranes into a 'smart' system with tuneable wettability, the use of polymeric thermoresponsive microgels is reported, as mentioned in the introduction.

3.3.1 Thermoresponsive microgels

PNIPAAm and PNIPAAm microgel with different AAc concentrations (6 and 10 wt.%) were prepared *via* surfactant-free emulsion polymerization (SFEP) in the presence of MBA crosslinking agent. Figure 3.12 shows the evolution of

hydrodynamic diameters (D_h) in a fixed range of temperatures (20 – 46ºC) of the prepared microgel samples. As observed from Figure 3.12 and stated in the literature [79], PNIPAAm microgels present a VPTT close to 30 – 32ºC. At room temperature microgels are in the swollen state, however their D_h sharply decreases above a critical temperature. At higher temperatures, the microgels have already collapsed and their diameters remain constant. When incorporating AAc in the system, the main goal was to induce a shift in the VPTT towards physiological conditions, in order to make the thermoresponsive microgels appropriate for future biomedical applications. In fact, the influence of AAc in the microgels' behaviour can be observed in both D_h and VPTT. Not only there is an increase in D_h with the increase of AAc content (235 to 455 nm at 20 ºC), but also there is a shift of the microgels' VPTT to higher temperatures with the addition of AAc (29 to 36ºC).

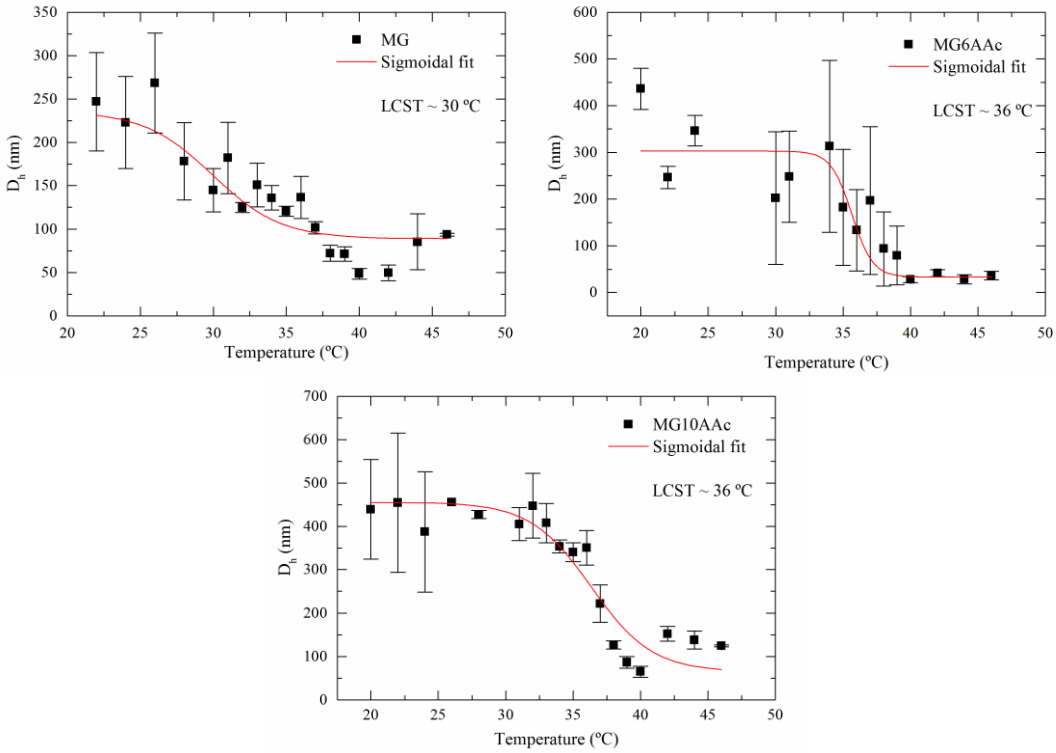

Figure 3.12 – Evolution of hydrodynamic diameter (Dh) with temperature for simple PNIPAAm microgels (MG), PNIPAAm microgels with 6 wt.% of AAc (MG6AAc) and PNIPAAm microgels with 10 wt.% of AAc (MG10AAc); variation of microgels' VPTT with adition of AAc.

By adding AAc to the PNIPAAm microgels' network, the electrostatic repulsions resulting from the new functional groups clash with the hydrophobic interactions (responsible for the microgels' network collapse). It is only by increasing the temperature that the hydrophobic interactions can overcome said electrostatic repulsions and cause the polymer network to fully collapse [80].

The size of the representative dried PNIPAAm microgels was measured with SEM (Figure 6.2, Section 6.7 of Supporting Information). As extracted from the micrograph, the microgels have a diameter of 32 ± 4 nm, which are smaller when compared to the hydrodynamic diameter measured in the collapsed state (approximately 50 nm). The observed difference can be explained considering the different states of the microgels and parameters measured, since DLS gives information regarding the hydrodynamic diameter that accounts for the diameter of particles plus a

layer of solvent where the particle (microgel) is moving, while SEM gives information about the diameter of the dried microgel.

3.3.2 Production of composite membranes

Considering the electrospinning optimization study made in Section 3.1.1 and the non-woven mats vs. films comparative study in Section 3.2, the best electrospinning parameters were selected to electrospun the composite membranes. The composite membranes were electrospun using colloidal electrospinning, since this is a cost-effective, simple and versatile technique that allows the production of polymeric fibres with other systems confined within them. This interesting characteristic enables the production of fibres with improved and tailored morphologies, depending on the desired application. Colloidal electrospinning is environmentally friendly since it enables the minimization of the amount of organic solvents used during the production process.

With the advantages of colloidal electrospinning in mind as well as the best electrospinning parameters chosen from the previously determined suitable range of conditions, the composite membranes were electrospun from a 14 wt.% PVP/EtOH solution with a 10% load of MG10AAc, using a flow rate of 0.7 $mL.h^{-1}$, an applied voltage of 15 kV and a TCD of 12 cm. Although 0.7 $mL.h^{-1}$ was not an obtained parameter on the electrospinning optimization study, it is well known that a decrease in flow rate leads to fibres with smaller diameters [72]. The decrease in process flow rate from 1 to 0.7 $mL.h^{-1}$ was made in order to bring the fibres' diameter closer to the microgels one. Another reason for the decrease in process flow rate is the presence of microgels in the solution. Since these particles can act as defects and generate inconsistencies in the fibre during electrospinning, the flow rate was decreased in order to maintain the observed monodisperse distribution of fibres diameters previously observed.

An UV treatment equal to the one made for the PVP membranes was applied to the composite membranes. SEM micrographs from the 5 and 60 minutes UV irradiated membranes are depicted in Figure 3.13. The respective MFD, as well as the remaining UV irradiated membranes (10, 15, 20, 30 and 40 minutes) can be consulted in Table 6.14 and Figure 6.3 on Section 6.8 of the Supporting Information.

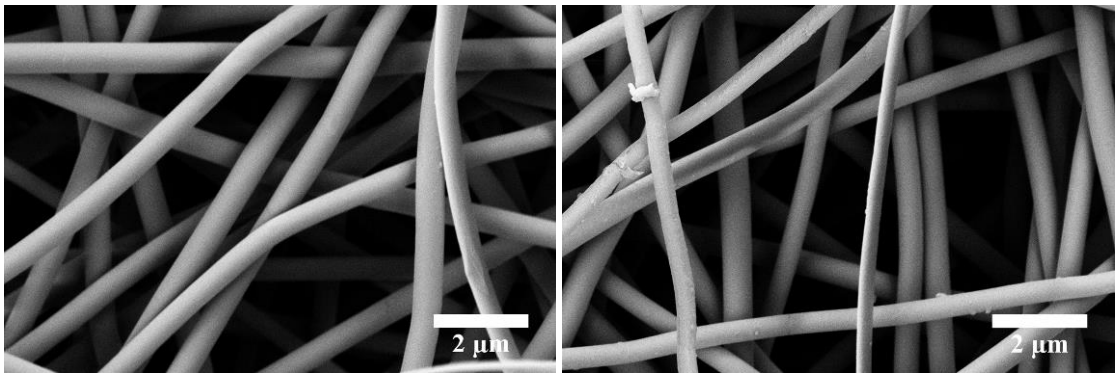

Figure 3.13 – SEM micrographs of composite UV crosslinked fibres for 5 (left) and 60 minutes (right). The micrographs were obtained using a 10k x magnification, a 5 kV electron beam, an aperture size of 30 µm and a WD of 5.8 mm.

Like it was observed in the PVP non-woven mats, no significant changes in the MFD of the composite membranes happened with the variation of the UV irradiation time (554 ± 64 nm for 5 minutes and 497 ± 78 nm for 60 minutes UV irradiation). The fibres show a smooth surface, as well as a narrow distribution of diameters (Figure 3.13). Comparing the MFD of the composite membranes with the ones obtained for the PVP non-woven mats, we see that

the composite membranes present a significant decrease in MFD. For instance, for a composite membrane irradiated for 60 minutes we obtained fibres with 497 ± 78 nm, while a PVP non-woven mat irradiated for 60 minutes presented a MFD of 817 ± 46 nm. Several factors could be influencing this harsh decrease. Firstly, and as mentioned before, the composite membranes were electrospun using a process flow rate of 0.7 $mL.h^{-1}$, which is smaller than the one used to electrospun the PVP non-woven mats (1 $mL.h^{-1}$). A lower flow rate will allow the solvent to have enough time to evaporate, being the end result fibres with lower diameter [17]. Also, with smaller flow rates the quantity of solution to be electrospun present in the tip of the needle is decreased. Since the applied voltage is the same and there is less mass of solution to be stretched, fibres with thinner diameters can be achieved.

Another parameter that may be responsible for the decrease in MFD is the solution's viscosity. In order to better understand the influence of this parameter, rheological studies were made to the solutions used in the electrospinning and colloidal electrospinning experiments. Both solutions had a fairly similar value of viscosity (3778.7 Pa.s for the 14 wt.% PVP/EtOH solution and 3023.3 Pa.s for the 10 wt.% MG10AAc @ 14 wt.% PVP/EtOH solution), which means that the viscosity is not an influencing parameter in the composite fibres' MFD.

Finally, a third parameter that may have caused the decrease of MFD in the composite fibres is the conductivity of the polymeric solution. This parameter is mainly determined by the polymer type, solvent used and the availability of ionisable salts [17]. In our case, the change in the solution's conductivity happened when the microgels were added to the 14 wt.% PVP/EtOH solution. Since the microgels had to be dispersed in water, the addition of this new solution to the PVP/EtOH increased the conductivity of the final solution [81]. Since both electrospinning and colloidal electrospinning solutions have a similar viscosity, the commanding factor on MFD decrease is the conductivity: a solution with higher conductivity has a higher charge density on the surface of the jet during electrospinning, which induces higher electrostatic repulsions between charges and consequently increased stretch of the polymeric jet (thinner fibres) [82].

Although it is not visible in SEM micrographs from Figure 3.13, the microgels were indeed confined into the PVP matrix as can be seen in TEM image (Figure 3.14). One explanation for the non-visualization of the microgels inside the fibres is the reduced diameter of microgels in comparison with the fibres diameter: 32 ± 4 nm against 497 ± 78 nm (60 minutes UV irradiation). Furthermore, the low amount of microgels incorporated within the fibres (10 wt.% regarding PVP weight) may not be enough to enable the visualization of the microgels.

ATR-FTIR measurements were carried out to evaluate the composition of the synthesized microgels and composite membranes. Figure 6.4 in Section 6.9 of the Supporting Information shows the spectra of PNIPAAm and PNIPAAm with 10 wt.% AAc microgels, as well as the spectrum for the composite membranes. Both the PNIPAAm based microgels spectra (MG and MG10AAc) present typical polyacrylamide transmittance bands at 3300 cm^{-1} (secondary amine), 1645 cm^{-1} (amide I), 1537 cm^{-1} (amide II) and 1456 cm^{-1}. As for the PVP, 3 typical transmission bands were detected: 1645 cm^{-1}, 1451 cm^{-1} and 1288 cm^{-1}.

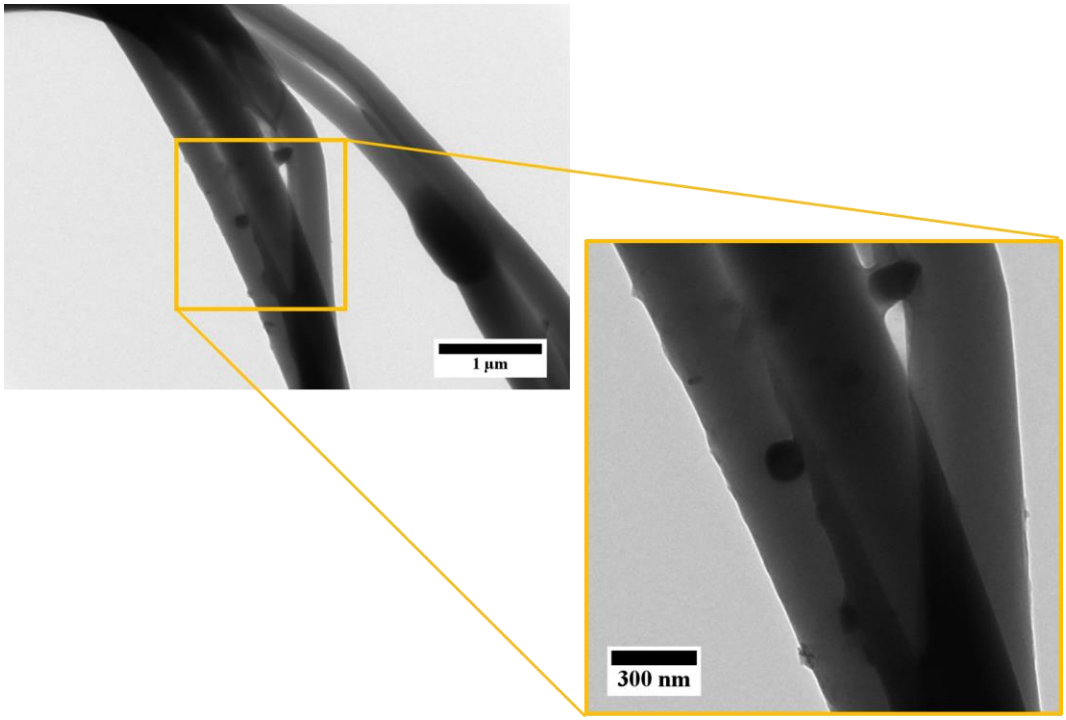

Figure 3.14 – TEM micrograph of PVP fibre with confined PNIPAAm-microgels.

3.3.3 Mechanical and swelling properties of composite membranes

In order to compare the composite membranes to the plain PVP membranes and films, both mechanical and swelling ratio tests were perform using the same conditions reported in Section 3.2: the composite membranes were cut into 10x5 mm samples and stretched with a speed of 0.1 $mm.min^{-1}$; for the swelling ratio tests, the membranes were also cut into 10x5 mm samples and immersed in water for 0.5, 1, 2, 3 and 5 h.

Regarding the mechanical properties of the composite membranes, Figure 3.15 shows the evolution of both Young's Modulus and UTS with the irradiation time. The correspondent values for Young's Modulus, UTS and elongation at break can be consulted in Table 6.15, available on Section 6.10 of Supporting Information. To better understand the microgels' influence, Figure 3.15 also shows the evolution of same parameters for the PVP non-woven mats.

As it happened for the PVP non-woven mats, the composite membranes reach an equilibrium state for the Young's Modulus after 20 minutes of irradiation time, once again indicating that 20 minutes seems to be enough time to crosslink the membranes and provide them stable mechanical properties. As for the influence of the confined microgels, it seems that it is not too evident through the mechanical properties: the composite membranes have a 'maximum' Young's Modulus of approximately 22 MPa, while for the PVP non-woven mats round the 25 MPa; the same happens for the UTS values (approximately 3.2 MPa for the composite membranes and 3.0 MPa for the PVP non-woven mats) (Figure 3.15). Once again, this lack of influence may be due to the reduced size of the microgels or to the insufficient load confined inside the PVP fibres.

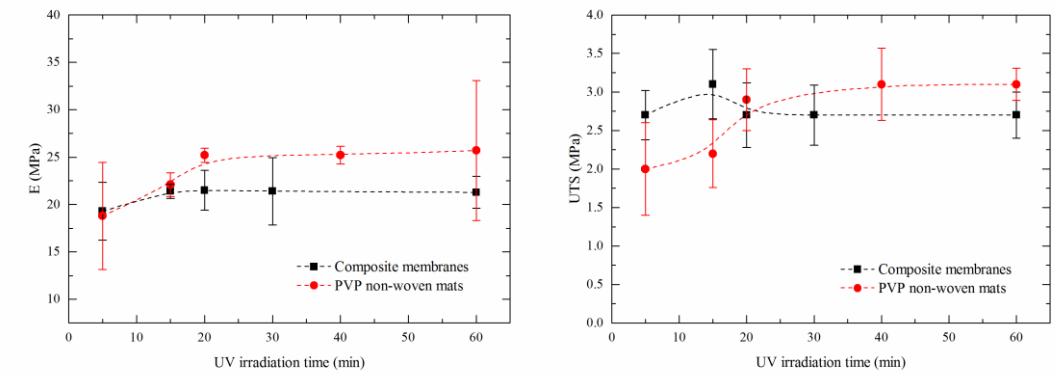

Figure 3.15 – Evolution of Young's Modulus (left graph) and UTS (right graph) with increasing irradiation time for composite membranes (square) *vs* PVP non-woven mats (circle).

The swelling properties of the composite membranes were tested to better comprehend the influence of the microgels in the composite membranes behaviour. Figure 3.16 shows the swelling ratio of the composite membranes as well as the respective mesh sizes and crosslinking density (complete values of mesh size and crosslinking density available on Table 6.17 at Section 6.11 of the Supporting Information). Two representative swelling ratio curves are also shown in order to facilitate the comparison between composite membranes and PVP non-woven mats.

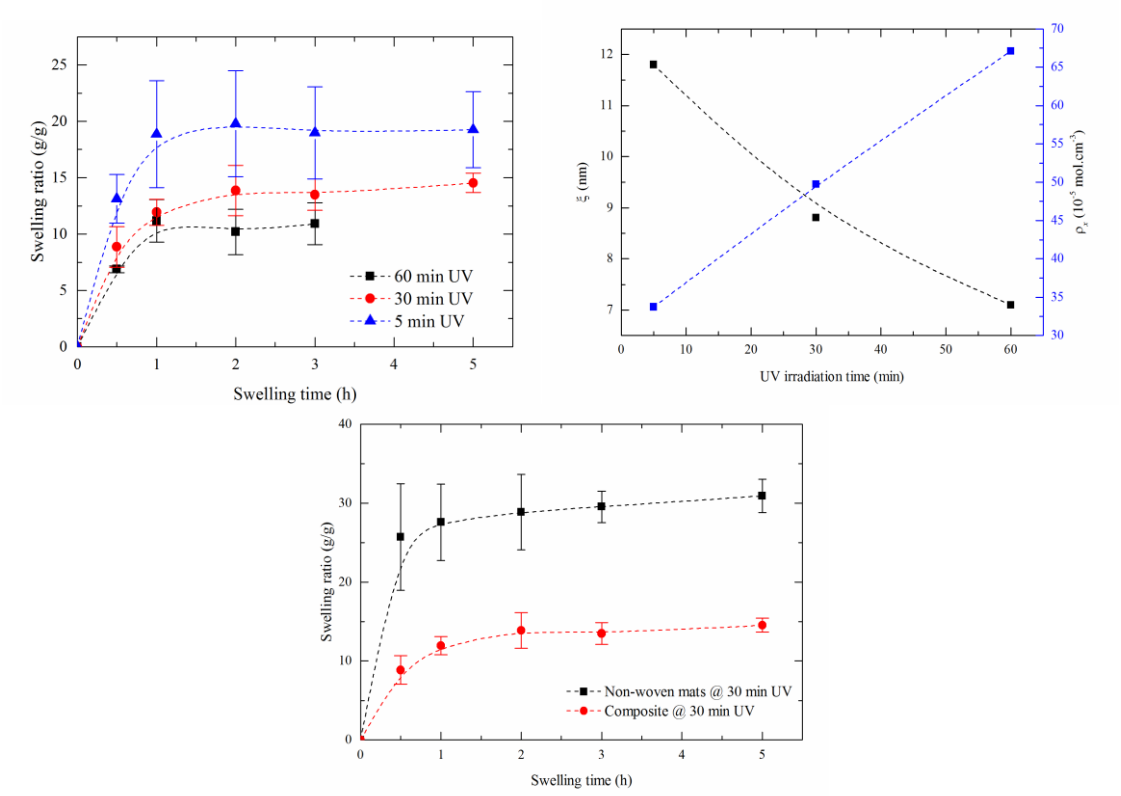

Figure 3.16 – Swelling ratio curves for UV crosslinked composite membranes with an irradiation period of 5 minutes (square), 30 minutes (circle) and 60 minutes (triangle). Variation of the membranes mesh size with varying UV irradiation times (right graph). Swelling ratio of PVP non-woven mats (bottom graph, squares) *vs* Composite membranes (bottom graph, circles) both UV irradiated for 30 minutes.

The composite membranes present a similar swelling behaviour to the PVP non-woven mats: with the increase of irradiation time there is a decrease in swelling capability. Once again, this difference is due to the higher crosslinking density presented by the membranes that were irradiated for a longer period of time (Figure 3.16, top right graph). Regarding the mesh size, the composite membranes present much smaller values when compared to the PVP non-woven mats (26 nm for a 5 minutes irradiated non-woven mat to 12 nm for a 5 minutes irradiated composite membrane). This difference of mesh size may be related to composite membranes' fibre diameter, which is smaller than the one for the PVP non-woven mats.

Interestingly the composite membranes present a much lower swelling ratio, at equilibrium, than the PVP non-woven mats (approximately 10 *vs.* 30, at 30 minutes of irradiation). This could be due to the confined microgels. Theoretically, when a fluid penetrates a network it chooses the path of least resistance to go from one side to the other, i.e. a straight line. In the composite membranes case, the addition of microgels creates obstacles (the microgels themselves) that interfere with the normal diffusion of water, forcing it to work around the obstacles. This means that the actual (average) path traversed by the species while diffusing in the interstitial fluid (in our case, water) in a porous medium (composite membranes) is longer than the path traversed in a solid medium (non-woven mats). Figure 3.17 depicts the effect of the confined microgels in the diffusion of a fluid, in this case water.

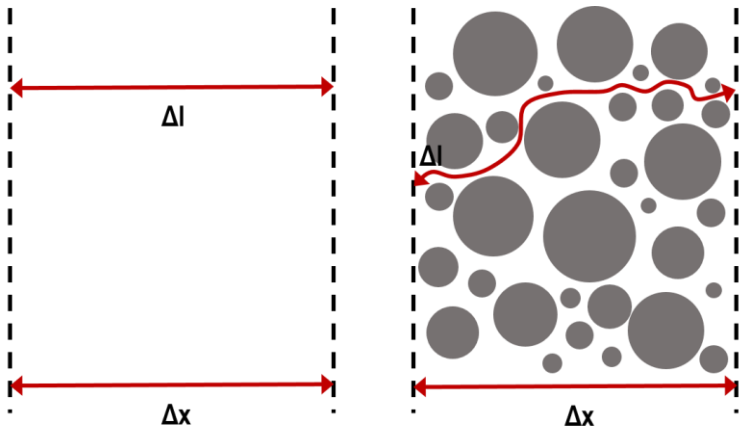

Figure 3.17 – Schematic representing the path of a fluid through a single fibre of an electrospun membrane *vs.* the path taken when particles (microgels) are confined inside the fibre. (Adapted from [83])

The ratio of the actual distance travelled by the species (Δl) per unit length of the medium (Δx) is commonly denominated as tortuosity [83], which is a parameter that strongly influences the diffusion coefficient of a fluid through a membrane. The relation between tortuosity and diffusion coefficient is presented in Eq. (3.6).

$$d_m^{'} = \frac{d_m}{\tau^2} \tag{3.6}$$

In Eq. (3.6) d'_m is the diffusion coefficient, d_m is the diffusion coefficient of the species in question in the fluid (water) without the presence of the 'obstacle' matrix (microgels) and τ the tortuosity. As it can be seen, the tortuosity is inversely proportional to the diffusion coefficient, which means that membranes with microgels (higher tortuosity) would have a lower diffusion coefficient and thus swell less than membranes with no confined microgels.

In order to create a membrane that can incorporate a certain amount of water and still be able to maintain a somewhat elastic behaviour, a commitment between structural stability, mechanical properties and swelling capability

needs to be taken into consideration. The most suitable studied UV irradiation time to produce such membrane would be 30 minutes, since samples with this irradiation time show mechanical properties identical to the ones that were irradiated for longer periods of time. Above 30 minutes of irradiation, the swelling properties are also fairly similar.

Although the confinement of microgels did not show a noticeable change in the mechanical properties of the membranes, changes in the swelling properties were evident. To further investigate the influence of the microgels, a higher load should be confined into the fibres, since with a 10 wt.% load (regarding PVP mass) the microgels are not homogeneously distributed throughout the entire membrane (Figure 3.14), which could be affecting the properties of the overall membrane.

4 Conclusions and Future Perspectives

This dissertation demonstrates the successful optimization of PVP as a fibre template for the production of composite membranes with confined thermoresponsive microgels as active sites. The applied UV irradiation treatment provided structure stability to the PVP non-woven mats in the presence of a solvent, preventing its dissolution. Consequently, hybrid fibrillary gels were successfully produced by colloidal electrospinning.

Firstly, PVP non-woven mats were produced using electrospinning technique. Four parameters that greatly influence the fibres' final diameter were studied: polymer concentration, process flow rate, applied voltage and target-to-collector distance. From this optimization study, it was possible to identify that polymer concentration and TCD had a higher influence on the fibres' MFD.

- The increase of polymer' concentration caused an increase in the MFD (585 ± 64 nm for 10 wt.% PVP/EtOH to 710 ± 97 nm for 14 wt.% PVP/EtOH). However, fibres electrospun from a solution with a polymer concentration of 10 wt.% presented either beads or fused fibres, and in some cases both phenomena were observed.
- Considering the influence of TCD, both tested distances (12 and 18 cm) proved to be suitable to form fibres, with 18 cm TCD showing a wider dispersion of diameters (400 – 1400 nm) than 12 cm TCD (550 – 850 nm).
- Finally, both the applied voltage values (10 and 15 kV), as well as the process flow rates tested (0.3 and 1 $mL.h^{-1}$) were able to successfully produce PVP electrospun fibres. Depending on the desired application and consequent MFD, one could use either values in both ranges.

Using those suitable conditions fibres with monodisperse distribution of diameter and a MFD between 585 and 825 nm were obtained.

The obtained non-woven mats were then crosslinked using UV irradiation (λ = 254 nm) in order to provide structural stability to PVP. The comparative study between non-woven mats and films showed that both cases present different behaviours when irradiated for different periods of time. Moreover, the irradiation time affected the properties of non-woven mats. Concerning the mechanical properties, above 20 minutes of irradiation the non-woven mats showed no remarkable differences in Young's Modulus and UTS values. This indicated that 20 minutes was enough irradiation time for the non-woven mat to be water insoluble and have a somewhat elastic behaviour. Higher irradiation times only have a higher impact in the fibres' morphology: cracks start to appear on the fibres surface after 60 minutes of irradiation, which can be an indicator of excessive UV exposure. Unlike non-woven mats, films did not present a stable mechanical behaviour within the studied range of irradiation times. In fact, when the applied irradiation time exceeded 5 h, photodegradation of PVP was observed. Therefore, it was not possible to draw any conclusion regarding this, since no stable structure was achieved with the studied PVP films.

As for the swelling properties, the non-woven mats presented a big difference between 5 and 30 minutes of irradiation (50 for 5 minutes of irradiation *vs.* 30 for 30 minutes of irradiation). This difference can be explained by crosslinking density (parameter obtained from the swelling properties). With an increase of irradiation time there is an increase in the crosslinking density of the formed network. At the same time the mobility of the polymeric chains could be hindered, which results in a lower uptake of water. Since there is no significant difference in swelling ratio

between the 30 and 60 minutes samples, and taking in consideration the mechanical properties' results, 30 minutes was determined as the most suitable irradiation time to crosslink the PVP non-woven mats.

After the electrospinning optimization process and the comparative study (non-woven mats *vs.* films), thermosensitive PNIPAAm based microgels were confined, which can act as active sites, into PVP non-woven mats using colloidal electrospinning to produce composite membranes. In order to produce the active site, copolymerization of AAc and NIPAAm monomers was performed obtaining microgels with a higher VPTT than PNIPAAm microgels. The increase in VPTT was successfully observed by DLS measurements, with PNIPAAm-AAc presenting a transition temperature at 36ºC in contrast with the temperature presented by PNIPAAm microgels (30ºC).

Interestingly, the composite membranes not only showed a lower mean fibre diameter than the PVP non-woven mats (497 ± 78 nm *vs* 817 ± 46 nm) but also a lower swelling capability (10 *vs.* 30; 30 minutes of irradiation). The difference of swelling capability could be attributed to the confined microgels, which could be acting as defects and consequently altering the diffusion path of water from a straight line to contouring line around the microgels (tortuosity effect). This could lead to a decrease in diffusion coefficient and thus a decrease in swelling capability. As for the mechanical properties, no remarkable differences were observed between the composite membranes and the PVP non-woven mats, most likely due to the low load of confined microgels used (10 wt.%, regarding PVP mass).

In summary, the main goal of this dissertation was achieved by optimizing PVP fibre template for the production of composite membranes containing thermoresponsive microgels as active sites. A range of parameters was successfully reached, in terms of composition, electrospun conditions and crosslinking, which guarantee the production of fibres with a monodisperse diameter distribution, as well as structure stability in the presence of a solvent. In the near future, it would be possible to create a versatile composite multifunctional system with tailored roughness and controlled responsiveness by optimization of the system in two main aspects:

(i) Improvement of microgel-to-fibre dimensions and concentration ratio: if the microgels have a diameter close to the fibre and are confined in concentrations higher than 10 wt.%, morphologies like 'bead-on-a-string' could be achieved.

(ii) Confinement of different active sites with different functionalities. This would allow to have, not only a control over the surface of the fibre, but also a control over the active sites (microgels), which would enable the use of this type of composite systems in controlled drug release applications. For instance, microgels with different stimuli-responsiveness could be confined into the polymeric matrix; microgels that respond to variations of magnetic field (incorporation of magnetic nanoparticles), or to light (incorporation of carbon nanotubes or gold nanoparticles) or even to changes in pH values.

This fibre template itself could also be further optimized, depending on the desired application. Design of Experiments (DoE) based on Responsive Surface Methodology (RSM) can be used to further explore the most suitable electrospinning parameters studied in this work, thus allowing the production of fibres with smaller diameters or tuneable wettability.

5 References

[1] D. Klinger and K. Landfester, "Photo-sensitive PMMA microgels: light-triggered swelling and degradation," *Soft Matter,* vol. 7, pp. 1426-1440, 2011.

[2] S. Bhattacharya, F. Eckert, V. Boyko, and A. Pich, "Temperature-, pH-, and magnetic-field-sensitive hybrid microgels," *Small,* vol. 3, pp. 650-7, Apr 2007.

[3] C. Echeverria, P. Soares, A. Robalo, L. Pereira, C. M. M. Novo, I. Ferreira, and J. P. Borges, "One-pot synthesis of dual-stimuli responsive hybrid PNIPAAm-chitosan microgels," *Materials & Design,* vol. 86, pp. 745-751, 2015.

[4] S. C. S. Marques, P. I. P. Soares, C. Echeveria, M. H. Godinho, and J. P. Borges, "Confinement of thermoresponsive microgels into fiber via colloidal electrospinning: experimental and statistical analysis," *RSC Adv.,* vol. 6, pp. 76370-76380, 2016.

[5] K. K. Chawla, *Composite Materials: Science and Engineering*, 3rd ed. New York: Springer, 2012.

[6] L. Ye, Y. Lu, Z. Su, and G. Meng, "Functionalized composite structures for new generation airframes: a review," *Composites Science and Technology,* vol. 65, pp. 1436-1446, 2005.

[7] J. Holbery and D. Houston, "Natural-Fiber-Reinforced Polymer Composites in Automotive Applications," *JOM,* pp. 80-86, 2006.

[8] A. Ashori, "Wood-plastic composites as promising green-composites for automotive industries!," *Bioresour Technol,* vol. 99, pp. 4661-7, Jul 2008.

[9] R. F. Gibson, "A review of recent research on mechanics of multifunctional composite materials and structures," *Composite Structures,* vol. 92, pp. 2793-2810, 2010.

[10] C. J. Ke, T. Y. Su, H. L. Chen, H. L. Liu, W. L. Chiang, P. C. Chu, Y. Xia, and H. W. Sung, "Smart multifunctional hollow microspheres for the quick release of drugs in intracellular lysosomal compartments," *Angew Chem Int Ed Engl,* vol. 50, pp. 8086-9, Aug 22 2011.

[11] J. S. Im, B. Bai, and Y. S. Lee, "The effect of carbon nanotubes on drug delivery in an electro-sensitive transdermal drug delivery system," *Biomaterials,* vol. 31, pp. 1414-9, Feb 2010.

[12] D. Y. Wu, S. Meure, and D. Solomon, "Self-healing polymeric materials: A review of recent developments," *Progress in Polymer Science,* vol. 33, pp. 479-522, 2008.

[13] E. Jo, S. Lee, K. T. Kim, Y. S. Won, H.-S. Kim, E. C. Cho, and U. Jeong, "Core-Sheath Nanofibers Containing Colloidal Arrays in the Core for Programmable Multi-Agent Delivery," *Advanced Materials,* vol. 21, pp. 968-972, 2009.

[14] Y.-J. Kim, M. Ebara, and T. Aoyagi, "A Smart Hyperthermia Nanofiber with Switchable Drug Release for Inducing Cancer Apoptosis," *Advanced Functional Materials,* vol. 23, pp. 5753-5761, 2013.

[15] R. James, S. G. Kumbar, C. T. Laurencin, G. Balian, and A. B. Chhabra, "Tendon tissue engineering: adipose-derived stem cell and GDF-5 mediated regeneration using electrospun matrix systems," *Biomed Mater,* vol. 6, p. 025011, Apr 2011.

[16] S. Agarwal, J. H. Wendorff, and A. Greiner, "Use of electrospinning technique for biomedical applications," *Polymer,* vol. 49, pp. 5603-5621, 2008.

[17] N. Bhardwaj and S. C. Kundu, "Electrospinning: a fascinating fiber fabrication technique," *Biotechnol Adv,* vol. 28, pp. 325-47, May-Jun 2010.

[18] Gisela Buschle-Diller, Andrew Hawkins, and J. Cooper, "Modified Fibers with Medical and Specialty Applications," ed Netherlands: Springer, 2006, pp. 67-80.

[19] M. Scampicchio, A. Bulbarello, A. Arecchi, M. S. Cosio, S. Benedetti, and S. Mannino, "Electrospun Nonwoven Nanofibrous Membranes for Sensors and Biosensors," *Electroanalysis,* vol. 24, pp. 719-725, 2012.

[20] D. G. Yu, X. X. Shen, C. Branford-White, K. White, L. M. Zhu, and S. W. Bligh, "Oral fast-dissolving drug delivery membranes prepared from electrospun polyvinylpyrrolidone ultrafine fibers," *Nanotechnology,* vol. 20, p. 055104, Feb 4 2009.

[21] A. J. Meinel, O. Germershaus, T. Luhmann, H. P. Merkle, and L. Meinel, "Electrospun matrices for localized drug delivery: current technologies and selected biomedical applications," *Eur J Pharm Biopharm,* vol. 81, pp. 1-13, May 2012.

[22] Z. Li and C. Wang, "Effects of Working Parameters on Electrospinning," pp. 15-28, 2013.

[23] D. Crespy, K. Friedemann, and A. M. Popa, "Colloid-electrospinning: fabrication of multicompartment nanofibers by the electrospinning of organic or/and inorganic dispersions and emulsions," *Macromol Rapid Commun,* vol. 33, pp. 1978-95, Dec 13 2012.

[24] A. L. Yarin, "Coaxial electrospinning and emulsion electrospinning of core-shell fibers," *Polymers for Advanced Technologies,* vol. 22, pp. 310-317, 2011.

[25] X. Li, Y. Su, S. Liu, L. Tan, X. Mo, and S. Ramakrishna, "Encapsulation of proteins in poly(L-lactide-co-caprolactone) fibers by emulsion electrospinning," *Colloids Surf B Biointerfaces,* vol. 75, pp. 418-24, Feb 1 2010.

[26] S. Agarwal and A. Greiner, "On the way to clean and safe electrospinning-green electrospinning: emulsion and suspension electrospinning," *Polymers for Advanced Technologies,* vol. 22, pp. 372-378, 2011.

[27] Honghu Qi, Ping Hu, Jun Xu, and A. Wang, "Encapsulation of Drug Reservoires in Fiber by Emulsion Electrospinning: Morphology Characterization and Preliminary release Assessment," *Biomacromolecules,* vol. 7, pp. 2327-2330, 2006.

[28] M. F. Elahi and W. Lu, "Core-shell Fibers for Biomedical Applications-A Review," *Journal of Bioengineering & Biomedical Science,* vol. 03, 2013.

[29] A. L. Yarin, S. Koombhongse, and D. H. Reneker, "Bending instability in electrospinning of nanofibers," *Journal of Applied Physics,* vol. 89, p. 3018, 2001.

[30] X. Xu, X. Zhuang, X. Chen, X. Wang, L. Yang, and X. Jing, "Preparation of Core-Sheath Composite Nanofibers by Emulsion Electrospinning," *Macromol Rapid Commun,* vol. 27, pp. 1637-1642, 2006.

[31] X. Xu, L. Yang, X. Wang, X. Chen, Q. Liang, J. Zeng, and X. Jing, "Ultrafine medicated fibers electrospun from W/O emulsions," *J Control Release,* vol. 108, pp. 33-42, Nov 2 2005.

[32] J. E. Díaz, A. Barrero, M. Márquez, A. Fernández-Nieves, and I. G. Loscertales, "Absorption Properties of Microgel-PVP Composite Nanofibers Made by Electrospinning," *Macromol Rapid Commun,* vol. 31, pp. 183-189, 2009.

[33] R. Pelton and T. Hoare, "Microgels and Their Synthesis: An Introduction," in *Microgels Suspensions: Fundamentals and Applications*, A. Fernandez-Nieves, H. M. Wyss, J. Mattsson, and D. A. Weitz, Eds., ed Weinheim: Wiley-VCH, 2011, pp. 3-32.

[34] M. Boularas, E. Gombart, J. F. Tranchant, L. Billon, and M. Save, "Design of smart oligo(ethylene glycol)-based biocompatible hybrid microgels loaded with magnetic nanoparticles," *Macromol Rapid Commun,* vol. 36, pp. 79-83, Jan 2015.

[35] A. S. Wadajkar, J. U. Menon, Y. S. Tsai, C. Gore, T. Dobin, L. Gandee, K. Kangasniemi, M. Takahashi, B. Manandhar, J. M. Ahn, J. T. Hsieh, and K. T. Nguyen, "Prostate cancer-specific thermo-responsive polymer-coated iron oxide nanoparticles," *Biomaterials,* vol. 34, pp. 3618-25, May 2013.

[36] V. Sundaresan, J. U. Menon, M. Rahimi, K. T. Nguyen, and A. S. Wadajkar, "Dual-responsive polymer-coated iron oxide nanoparticles for drug delivery and imaging applications," *Int J Pharm,* vol. 466, pp. 1-7, May 15 2014.

[37] C. Liu, C. Yao, Y. Zhu, J. Ren, and L. Ge, "Dually responsive one dimensional photonic crystals with reversible color changes," *Sensors and Actuators B: Chemical,* vol. 220, pp. 227-232, 2015.

[38] Y. Qin, J. Chen, Y. Bi, X. Xu, H. Zhou, J. Gao, Y. Hu, Y. Zhao, and Z. Chai, "Near-infrared light remote-controlled intracellular anti-cancer drug delivery using thermo/pH sensitive nanovehicle," *Acta Biomater,* vol. 17, pp. 201-9, Apr 2015.

[39] A. K. Teotia, H. Sami, and A. Kumar, *Switchable and Responsive Surfaces and Materials for Biomedical Applications*, 2015.

[40] Y. Qiu and K. Park, "Environment-sensitive hydrogels for drug delivery," *Adv Drug Deliv Rev,* vol. 53, pp. 321-39, Dec 31 2001.

[41] M. K. Jaiswal, R. Banerjee, P. Pradhan, and D. Bahadur, "Thermal behavior of magnetically modalized poly(N-isopropylacrylamide)-chitosan based nanohydrogel," *Colloids Surf B Biointerfaces,* vol. 81, pp. 185-94, Nov 1 2010.

[42] B. R. Saunders, "On the structure of poly(N-isopropylacrylamide) microgel particles," *Langmuir,* vol. 20, pp. 3925-32, May 11 2004.

[43] M. Constantin, "Lower critical solution temperature versus volume phase transition temperature in thermoresponsive drug delivery systems," *Express Polymer Letters,* vol. 5, pp. 839-848, 2011.

[44] K. Van Durme, H. Rahier, and B. Van Mele, "Influence of Additives on the Thermoresponsive Behavior of Polymers in Aqueous Solution," *Macromolecules,* vol. 38, pp. 10155-10163, 2005.

[45] A. Burmistrova and R. von Klitzing, "Control of number density and swelling/shrinking behavior of P(NIPAM-AAc) particles at solid surfaces," *Journal of Materials Chemistry,* vol. 20, pp. 3502-3507, 2010.

[46] K. C. Johnson, F. Mendez, and M. J. Serpe, "Detecting solution pH changes using poly (N-isopropylacrylamide)-co-acrylic acid microgel-based etalon modified quartz crystal microbalances," *Anal Chim Acta,* vol. 739, pp. 83-8, Aug 20 2012.

[47] M. Das, N. Sanson, D. Fava, and E. Komacheva, "Microgels Loaded with Gold Nanorods: Photothermally Triggered Volume Transitions und Physiological Conditions," *Langmuir,* vol. 23, pp. 196-201, 2007.

[48] J. D. Debord and L. A. Lyon, "On the unusual stability of succinimidyl esters in pNIPAm-AAc microgels," *Bioconjug Chem,* vol. 18, pp. 601-4, Mar-Apr 2007.

[49] O. Wichterle and D. Lim, "Hydrophilic Gels for Biological Use," *Nature,* vol. 185, pp. 117-118, 1960.
[50] A. S. Hoffman, "Applications of thermally reversible polymers and hydrogels in therapeutics and diagnostics," *Journal of Controlled Release,* vol. 6, pp. 297-305, 1987.
[51] C. M. S. Hassan, Jennifer E.; Peppas, Nikolaos A., "Diffusional characteristics of freeze/thawed poly(vynil alcohol) hydrogels: Applications to protein controlled release from multilaminate devices," *European Journal of Pharmaceutics and Biopharmaceutics,* vol. 49, pp. 161-165, 2000.
[52] K. T. Nguyen and J. L. West, "Photopolymerizable hydrogels for tissue engineering applications," *Biomaterials,* vol. 23, pp. 4307-14, Nov 2002.
[53] J. L. Drury and D. J. Mooney, "Hydrogels for tissue engineering: scaffold design variables and applications," *Biomaterials,* vol. 24, pp. 4337-51, Nov 2003.
[54] Y. Li, J. Rodrigues, and H. Tomas, "Injectable and biodegradable hydrogels: gelation, biodegradation and biomedical applications," *Chem Soc Rev,* vol. 41, pp. 2193-221, Mar 21 2012.
[55] N. A. B. Peppas, P.; Leobandung, W.; Ichikawa, H., "Hydrogels in pharmaceutical formulations," *European Journal of Pharmaceutics and Biopharmaceutics,* vol. 50, pp. 27-46, 2000.
[56] S. Van Vlierberghe, P. Dubruel, and E. Schacht, "Biopolymer-based hydrogels as scaffolds for tissue engineering applications: a review," *Biomacromolecules,* vol. 12, pp. 1387-408, May 9 2011.
[57] A. S. Hoffman, "Hydrogels for biomedical applications," *Advanced Drug Delivery Reviews,* vol. 64, pp. 18-23, Dec 2012.
[58] L. C. Lopérgolo, A. B. Lugão, and L. H. Catalani, "Direct UV photocrosslinking of poly(N-vinyl-2-pyrrolidone) (PVP) to produce hydrogels," *Polymer,* vol. 44, pp. 6217-6222, 2003.
[59] G. D'Errico, M. De Lellis, G. Mangiapia, A. Tedeschi, O. Ortona, S. Fusco, A. Borzacchiello, and L. Ambrosio, "Structural and mechanical properties of UV-photo-cross-linked poly(N-vinyl-2-pyrrolidone) hydrogels," *Biomacromolecules,* vol. 9, pp. 231-40, Jan 2008.
[60] X. F. Zhu, P. Lu, W. Chen, and J. A. Dong, "Studies of UV crosslinked poly(N-vinylpyrrolidone) hydrogels by FTIR, Raman and solid-state NMR spectroscopies," *Polymer,* vol. 51, pp. 3054-3063, Jun 24 2010.
[61] G. P. Kumar, A. R. Phani, R. G. Prasad, J. S. Sanganal, N. Manali, R. Gupta, N. Rashmi, G. S. Prabhakara, C. P. Salins, K. Sandeep, and D. B. Raju, "Polyvinylpyrrolidone oral films of enrofloxacin: film characterization and drug release," *Int J Pharm,* vol. 471, pp. 146-52, Aug 25 2014.
[62] D. A. Carr and N. A. Peppas, "Molecular structure of physiologically-responsive hydrogels controls diffusive behavior," *Macromol Biosci,* vol. 9, pp. 497-505, May 13 2009.
[63] A. P. S. Immich, P. H. H. de Araujo, L. H. Catalani, A. A. U. de Souza, and S. M. A. G. U. Souza, "Crosslinking of Poly(N-vinyl-2-pyrrolidone) in the Coating of Cotton Yarn," *Polymer Engineering and Science,* vol. 51, pp. 445-453, Mar 2011.
[64] J. Rosiak, J. Oleiniczak, and W. Pekala, "Fast reaction of irradiated polymers - I. Crosslinking and degradation of polyvinylpyrrolidone," *Radiation Physics and Chemistry,* vol. 36, pp. 747-755, 1990.
[65] Q. G. Zhang, W. W. Hu, A. M. Zhu, and Q. L. Liu, "UV-crosslinked chitosan/polyvinylpyrrolidone blended membranes for pervaporation," *Rsc Advances,* vol. 3, pp. 1855-1861, 2013.
[66] D. Lubasova, H. Niu, X. Zhao, and T. Lin, "Hydrogel properties of electrospun polyvinylpyrrolidone and polyvinylpyrrolidone/poly(acrylic acid) blend nanofibers," *RSC Adv.,* vol. 5, pp. 54481-54487, 2015.
[67] M. Goldberg, R. Langer, and X. Jia, "Nanostructured materials for applications in drug delivery and tissue engineering," *Journal of Biomaterials Science, Polymer Edition,* vol. 18, pp. 241-268, 2007.
[68] B. V. Slaughter, S. S. Khurshid, O. Z. Fisher, A. Khademhosseini, and N. A. Peppas, "Hydrogels in regenerative medicine," *Adv Mater,* vol. 21, pp. 3307-29, Sep 4 2009.
[69] J. Zhu and R. E. Marchant, "Design properties of hydrogel tissue-engineering scaffolds," *Expert Rev Med Devices,* vol. 8, pp. 607-26, Sep 2011.
[70] H. M. Crowther and B. Vincent, "Swelling behavior of poly N-isopropylacrylamide microgel particles in alcoholic solutions," *Colloid and Polymer Science,* vol. 276, pp. 46-51, Jan 1998.
[71] S. De Vrieze, T. Van Camp, A. Nelvig, B. Hagström, P. Westbroek, and K. De Clerck, "The effect of temperature and humidity on electrospinning," *Journal of Materials Science,* vol. 44, pp. 1357-1362, 2008.
[72] S. Agarwal, A. Greiner, and J. H. Wendorff, "Functional materials by electrospinning of polymers," *Progress in Polymer Science,* vol. 38, pp. 963-991, 2013.
[73] F. E. Ahmed, B. S. Lalia, and R. Hashaikeh, "A review on electrospinning for membrane fabrication: Challenges and applications," *Desalination,* vol. 356, pp. 15-30, 2015.
[74] T. J. Sill and H. A. von Recum, "Electrospinning: applications in drug delivery and tissue engineering," *Biomaterials,* vol. 29, pp. 1989-2006, May 2008.
[75] T. E. Newsome and S. V. Olesik, "Electrospinning Silica/Polyvinylpyrrolidone Composite Nanofibers," *Journal of Applied Polymer Science,* vol. 131, pp. 1-9, Nov 5 2014.

[76] M. Chen, H. Qu, J. Zhu, Z. Luo, A. Khasanov, A. S. Kucknoor, N. Haldolaarachchige, D. P. Young, S. Wei, and Z. Guo, "Magnetic electrospun fluorescent polyvinylpyrrolidone nanocomposite fibers," *Polymer,* vol. 53, pp. 4501-4511, 2012.

[77] A. Sionkowska, M. Wisniewski, J. Skopinska, S. Vicini, and E. Marsano, "The influence of UV irradiation on the mechanical properties of chitosan/poly(vinyl pyrrolidone) blends," *Polymer Degradation and Stability,* vol. 88, pp. 261-267, May 2005.

[78] P. J. Flory and J. Rehner, "Statistical Mechanics of Cross-Linked Polymer Networks I. Rubberlike Elasticity," *The Journal of Chemical Physics,* vol. 11, p. 512, 1943.

[79] L. E. Strong and J. L. West, "Thermally responsive polymer-nanoparticle composites for biomedical applications," *Wiley Interdiscip Rev Nanomed Nanobiotechnol,* vol. 3, pp. 307-17, May-Jun 2011.

[80] A. Burmistrova, M. Richter, M. Eisele, C. Üzüm, and R. von Klitzing, "The Effect of Co-Monomer Content on the Swelling/Shrinking and Mechanical Behaviour of Individually Adsorbed PNIPAM Microgel Particles," *Polymers,* vol. 3, pp. 1575-1590, 2011.

[81] P. Q. Franco, C. F. C. João, J. C. Silva, and J. P. Borges, "Electrospun hydroxyapatite fibers from a simple sol–gel system," *Materials Letters,* vol. 67, pp. 233-236, 2012.

[82] M. Ignatova, N. Manolova, and I. Rashkov, "Electrospinning of poly(vinyl pyrrolidone)–iodine complex and poly(ethylene oxide)/poly(vinyl pyrrolidone)–iodine complex – a prospective route to antimicrobial wound dressing materials," *European Polymer Journal,* vol. 43, pp. 1609-1623, 2007.

[83] L. Shen and Z. Chen, "Critical review of the impact of tortuosity on diffusion," *Chemical Engineering Science,* vol. 62, pp. 3748-3755, 2007.

[84] C. M. Schilli, M. Zhang, E. Rizzardo, S. H. Thang, B. Y. K. Chong, K. Edwards, G. Karlsson, and A. H. E. Müller, "A new double-responsive block copolymer synthesized via RAFT polymerization: Poly(*N*-isopropylacrylamide)-*block*-poly(acrylic acid)," *Macromolecules,* vol. 37, pp. 7861-7866, 2004.

6 Supporting Information

6.1 Conditions for the synthesis of PNIPAAm based microgels and respective hydrodynamic diameters

Table 6.1 – Reagents and respective quantities used to produce PNIPAAm microgels.

Reagents	wt.% monomer	Mass (g)	Volume (mL)
NIPAAm	100	1	20
MBA	5	0.05	20
APS	10	0.1	20
SBS	5	0.05	20
			80 + 20 mL H_2O

Since acrylic acid comes in liquid form and its density is 1.05 $g.cm^{-3}$, upon synthesis of PNIPAAm-AAc microgels the volume of AAc corresponding to 6 and 10 wt.% (regarding PVP mass) is 57.1 and 95.2 µL, respectively.

Table 6.2 – Hydrodynamic and polydispersion index values for synthesized microgels measured by DLS at 24 and 40ºC. All measurements were performed at pH 5.6

Sample	24ºC		40ºC	
	D_h (nm)	PI	D_h (nm)	PI
MG	223 ± 53	0.97	48 ± 6.3	0.34
MG6AAc	346 ± 32	0.68	28 ± 6.4	0.43
MG10AAc	387 ± 139	1.07	65 ± 12	0.32

6.2 MFD values resulting from electrospinning optimization study

Table 6.3 – MFD for all variations done during the electrospinning optimization study.

Concentration (wt.%)	Flow rate ($mL.h^{-1}$)	Applied voltage (kV)	TCD (cm)	MFD (nm)
10	0.3	10	12	1072 ± 551
			18	----------[a]
		15	12	562 ± 85[b]
			18	585 ± 64b
	1.0	10	12	1028 ± 201b
			18	896 ± 151
		15	12	862 ± 122
			18	862 ± 120
14	0.3	10	12	787 ± 156
			18	888 ± 179
		15	12	710 ± 97
			18	1015 ± 672[c]
	1.0	10	12	1695 ± 239[d]
			18	1653 ± 330d
		15	12	1482 ± 175
			18	1351 ± 175d

[a] Fibres presented beads, fusion and polydisperse distribution
[b] Fibres presented beads
[c] Fibres presented slight polydisperse distribution
[d] Fibres presented striations, possibly due to some defect on the needle

6.3 SEM micrographs of PVP fibres and respective MFDs

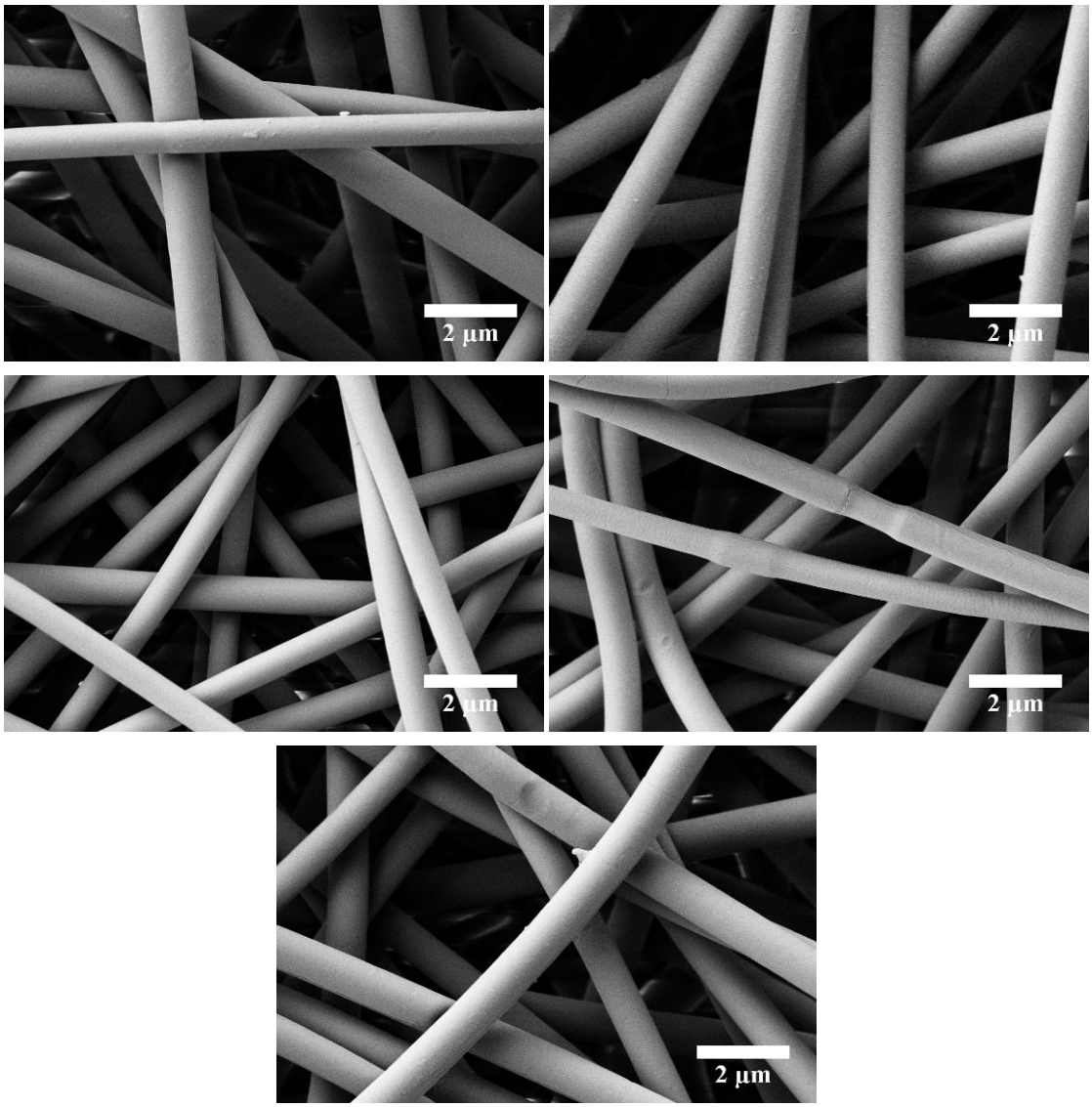

Figure 6.1 – SEM micrographs of PVP UV crosslinked fibres for 10 minutes (top left), 15 minutes (top right), 20 minutes (middle left), 30 minutes (middle right) and 40 minutes (bottom). The micrographs were obtained using a 10k x magnification, a 5 kV electron beam, an aperture size of 30 µm and a WD of 5.8 mm.

Table 6.4 – PVP fibres MFD with variation of UV irradiation time.

UV irradiation (min)	MFD (nm)
5	823 ± 50
10	856 ± 111
15	833 ± 69
20	665 ± 49
30	741 ± 82
40	871 ± 64
60	817 ± 46

6.4 Mechanical tests results for PVP films and non-woven mats

Table 6.5 – Tensile tests results for each PVP film's UV irradiation time.

Shear	UV irradiation (h)	*E* (MPa)	UTS (MPa)	*ε* (%)
Parallel	1	346 ± 80.1	12.1 ± 2.86	0.67 ± 0.14
	2	1070 ± 90.87	77.1 ± 8.37	1.99 ± 0.372
	5	1950 ± 347.6	96.5 ± 7.51	1.29 ± 0.481
Perpendicular	1	383 ± 49.2	13.1 ± 1.32	0.68 ± 0.27
	2	1053 ± 218.0	84.8 ± 5.88	2.49 ± 0.757
	5	1960 ± 86.29	95.2 ± 9.13	0.89 ± 0.44

Table 6.6 – Tensile tests results for each PVP non-woven mats' UV irradiation time.

UV irradiation (min)	*E* (MPa)	UTS (MPa)	*ε* (%)
5	18.8 ± 5.65	2.0 ± 0.6	30.2 ± 19.2
15	22.1 ± 1.25	2.2 ± 0.44	30.7 ± 11.0
20	25.2 ± 0.73	2.9 ± 0.40	55.4 ± 9.54
40	25.2 ± 0.94	3.1 ± 0.47	39.4 ± 17.2
60	25.7 ± 7.39	3.1 ± 0.21	32.3 ± 10.9

6.5 Molecular weight of the polymer chain between two neighbouring crosslinking nodes, mesh size and crosslinking density for PVP films

Table 6.7 – $v_{2,s}$ at different swelling times for PVP film samples in shear's parallel direction.

UV irradiation (h)	0.5 h swelling time	1 h swelling time	2 h swelling time	3 h swelling time	5 h swelling time	8 h swelling time
3	0.0241 ± 0.0021	0.0243 ± 0.0036	0.0328 ± 0.0101	0.0264 ± 0.0075	0.0528 ± 0.002	----------
2	0.0340 ± 0.0048	0.0306 ± 0.0011	0.0476 ± 0.0091	0.0432 ± 0.011	0.0457 ± 0.0095	----------
1	0.0312 ± 0.0024	0.0311 ± 0.0005	0.0321 ± 0.0063	0.0274 ± 0.0034	0.0326 ± 0.0022	0.0313 ± 0.0087

Table 6.8 – $v_{2,s}$ at different swelling times for PVP film samples in shear's perpendicular direction.

UV irradiation (h)	0.5 h swelling time	1 h swelling time	2 h swelling time	3 h swelling time	5 h swelling time	8 h swelling time
3	0.0293 ± 0.0036	0.0281 ± 0.0069	0.0284 ± 0.0011	0.0306 ± 0.0032	0.0465 ± 0.002	----------
2	0.0304 ± 0.0101	0.0310 ± 0.0057	0.0328 ± 0.0021	0.0326 ± 0.0097	0.0402 ± 0.0061	----------
1	0.0391 ± 0.0046	0.0285 ± 0.0048	0.0308 ± 0.0016	0.0319 ± 0.0049	0.0367 ± 0.0093	0.0371 ± 0.0071

Table 6.9 – Variation of the molecular weight of the polymer between two neighbouring crosslinking nodes with the UV irradiation time and swelling time for PVP films.

Swelling time (h)	$\overline{M}_c$ (Da)					
	Parallel			Perpendicular		
	3 h UV	2 h UV	1 h UV	3 h UV	2 h UV	1 h UV
0.5	7785	5356	6087	6151	6415	4779
1	7728	5983	6098	6420	6305	6688
2	5696	3691	5901	6348	5943	6165
3	7123	4130	6954	5880	5982	5953
5	3348	3867	5810	3730	4767	5123
8	----------	----------	6061	----------	----------	5065

Table 6.10 – Variation of the mesh size with the UV irradiation time and swelling time of PVP films.

Swelling time (h)	ξ (nm)					
	Parallel			Perpendicular		
	3 h UV	2 h UV	1 h UV	3 h UV	2 h UV	1 h UV
0.5	22.1	16.4	17.9	18.4	18.6	14.7
1	21.9	17.9	17.9	19.0	18.3	19.4
2	17.1	12.1	17.5	18.9	17.4	18.1
3	20.5	13.2	20.0	17.7	17.5	17.6
5	11.2	12.6	17.3	12.3	14.6	15.6
8	----------	----------	17.9	----------	----------	15.4

Table 6.11 – Variation of the crosslinking density with the UV irradiation time and swelling time of PVP films.

Swelling time (h)	ρ_x (10^{-5} mol.cm^{-3})					
	Parallel			Perpendicular		
	3 h UV	2 h UV	1 h UV	3 h UV	2 h UV	1 h UV
0.5	16.1	23.3	20.5	20.3	19.5	26.2
1	16.3	20.9	20.5	19.5	19.8	18.7
2	21.9	33.9	21.2	19.7	21.0	20.3
3	17.5	30.3	18.0	21.3	20.9	21.0
5	37.3	32.3	21.5	33.5	26.2	24.4
8	----------	----------	20.6	----------	----------	24.7

6.6 Molecular weight of the polymer chain between two neighbouring crosslinking nodes, mesh size and crosslinking density for PVP non-woven mats

Table 6.12 – Variation of the molecular weight of the polymer between two neighbouring crosslinking nodes for PVP non-woven mats.

Swelling time (h)	$\overline{M}_c$ (Da)		
	60 min UV	30 min UV	5 min UV
0.5	3025	5230	7247
1	4216	5862	9934
2	4118	6145	10102
3	4723	6468	10168
5	4640	6767	9867

Table 6.13 – Variation of the mesh size and crosslinking density with the UV irradiation time and swelling time for PVP non-woven mats.

Swelling time (h)	ξ (nm)			ρ_x (10^{-5} mol.cm^{-3})		
	60 min UV	30 min UV	5 min UV	60 min UV	30 min UV	5 min UV
0.5	10.1	15.3	20.4	41.3	23.9	17.2
1	12.9	16.8	26.6	29.6	21.3	12.6
2	12.8	17.4	27.0	30.3	20.3	12.4
3	14.2	18.2	27.2	26.5	19.3	12.3
5	14	18.9	26.5	26.9	18.5	12.7

6.7 SEM micrograph of dried PNIPAAm microgels

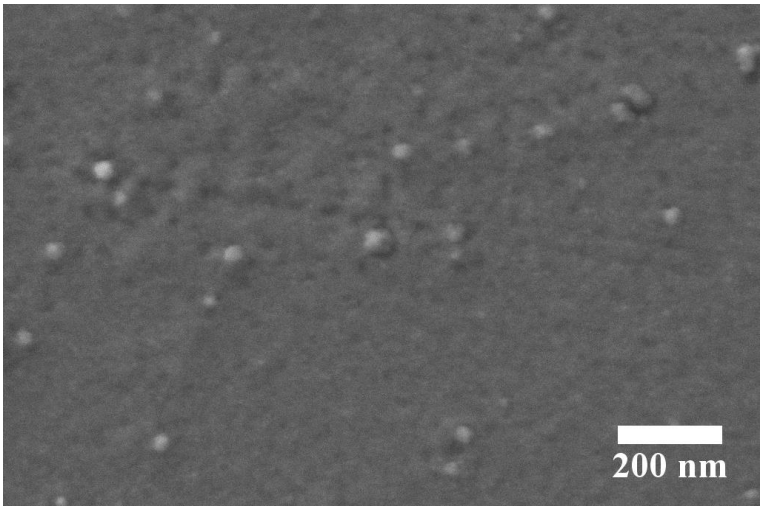

Figure 6.2 – SEM micrograph of PNIPAAm microgels.

6.8 SEM micrographs of composite membranes and respective MFD

Table 6.14 – Composite fibres MFD with variation of UV irradiation time.

UV irradiation (min)	MFD (nm)
5	554 ± 64
10	511 ± 65
15	579 ± 109
20	543 ± 69
30	532 ± 45
40	509 ± 60
60	497 ± 78

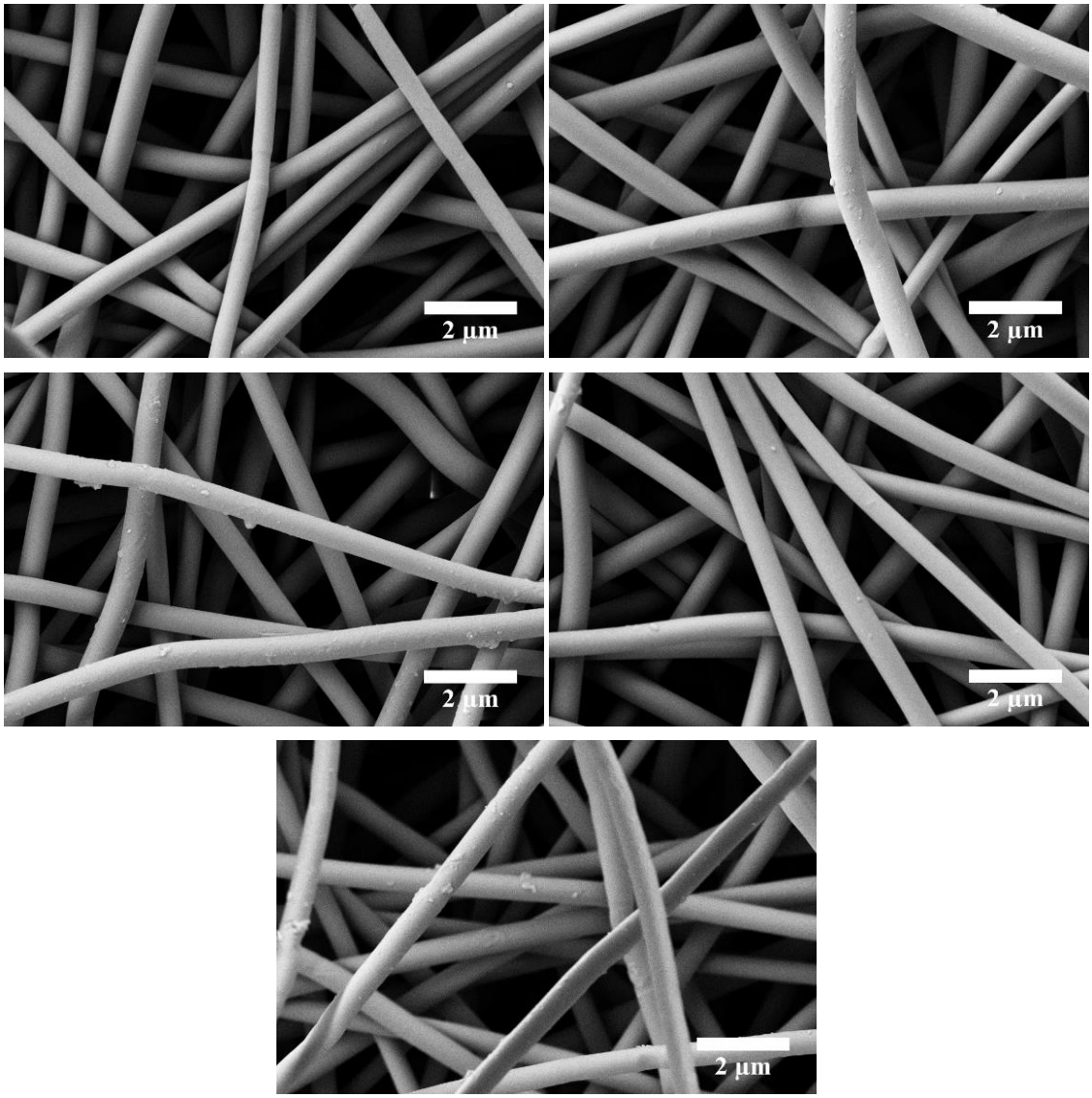

Figure 6.3 – SEM micrographs of composite UV crosslinked fibres for 10 minutes (top left), 15 minutes (top right), 20 minutes (middle left), 30 minutes (middle right) and 40 minutes (bottom). The micrographs were obtained using a 10k x magnification, a 5 kV electron beam, an aperture size of 30 µm and a WD of 5.8 mm.

6.9 ATR-FTIR analysis of the composite membranes

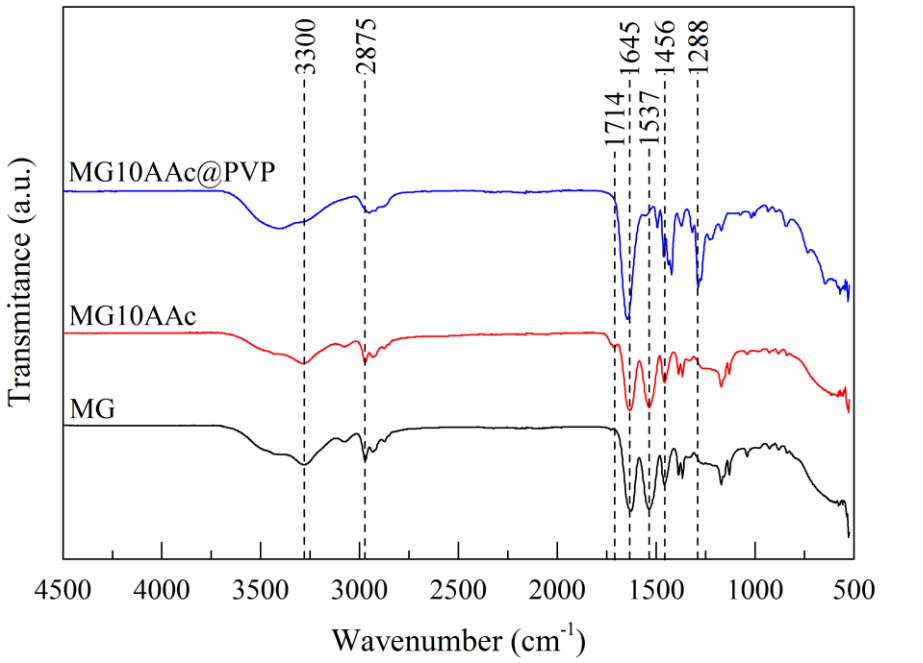

Figure 6.4 – ATR-FTIR spectra of PNIPAAm microgels (black), PNIPAAm microgels with 10 wt.% of AAc (red) and PVP fibres with incorporated 10 wt.% AAc/PNIPAAm microgels (blue).

The band vibration amide I (1645 cm^{-1}) is assigned to the stretching of the C=O bond, while amide II vibration corresponds to the stretching of -NH bond. As for the 3300 and the 1456 cm^{-1} transmittance bands, the first is related to the stretching a N-H bond while the last arises from the deformation of δ(-CH_3) and δ(-CH2) groups [41]. In the MG10AAc it is possible to see a faint transmittance band appearing at 1714 cm^{-1}, which arises from C=O stretching of the acrylic acid –COOH groups [84]. Regarding the composite membranes, some of its transmittance bands are overlapped with the PNIPAAm microgels ones. For instance, at 1645 cm^{-1} (amide I of the PNIPAAm based microgels), the composite membranes present a transmittance band relative to the combined contribution from C=O and C-N stretching of PVP [66]. Another two bands related to the PVP appear in the composite membranes' spectrum: 1451 cm^{-1} and 1288 cm^{-1}, with the first one being a combination of three different factors (wag of the CH_2 ring, stretch of the C-N ring and bending of C-H in the methine group) and the second one a combination of C-N stretch and CH_2 ring wag. It is important to refer that all the samples present a transmittance band at 2875 cm^{-1}: stretching of CH, CH_2 and CH_3.

6.10 Composite membranes' mechanical test results

Table 6.15 – Tensile tests results for each composite membrane's UV irradiation time.

UV irradiation (min)	*E* (MPa)	UTS (MPa)	*ε* (%)
5	19.3 ± 3.06	2.7 ± 0.32	35.5 ± 1.97
15	21.4 ± 0.73	3.1 ± 0.45	32.3 ± 1.97
20	21.5 ± 2.10	2.7 ± 0.42	29.6 ± 5.99
30	21.4 ± 3.56	2.7 ± 0.39	30.2 ± 7.22
60	21.3 ± 1.68	2.7 ± 0.30	26.5 ± 4.18

6.11 Molecular weight of the polymer chain between two neighbouring crosslinking nodes and mesh size for composite membranes

Table 6.16 – Variation of the molecular weight of the polymer between two neighbouring crosslinking nodes for composite membranes.

Swelling time (h)	$\overline{M}_c$ (Da)		
	60 min UV	30 min UV	5 min UV
0.5	1060	1432	2435
1	1925	2173	3619
2	1690	2553	3822
3	1863	2516	3704
5	----------	2773	3818

Table 6.17 – Variation of the mesh size and crosslinking density with the UV irradiation time and swelling time for composite membranes.

Swelling time (h)	ξ (nm)			ρ_x (10^{-5} mol.cm^{-3})		
	60 min UV	30 min UV	5 min UV	60 min UV	30 min UV	5 min UV
0.5	4.7	5.8	8.6	117.9	87.3	51.3
1	7.2	7.9	11.6	64.9	57.5	34.5
2	6.6	8.9	12.1	73.9	48.9	32.7
3	7.1	8.8	11.8	67.1	49.7	33.7
5	----------	9.5	12.1	----------	45.1	32.7